Uncommon lanthanide ions in purely 4f Single Molecule Magnets

Fabrice Pointillart, O. Cador, Boris Le Guennic, L. Ouahab

Edited Dec 26

Uncommon Lanthanide Ions in Purely 4*f* Single Molecule Magnets

Fabrice Pointillart,[*,1] Olivier Cador,[1] Boris Le Guennic,[1] Lahcène Ouahab[1]

[1] *Institut des Sciences Chimiques de Rennes, UMR 6226 CNRS - Université de Rennes 1, 263 Avenue du Général Leclerc 35042 Rennes Cedex (France)*

Contents

1. Introduction....3
1. Mononuclear Ytterbium SMMs....5
2. Polynuclear Ytterbium SMMs....16
3. SMMs built from other uncommon lanthanide ions....23
   3.1. Cerium SMMs....23
   3.2. Neodymium SMMs....26
   3.3. Holmium SMMs....31
   3.4. Thulium SMM....35
4. Heterobinuclear Zinc-Lanthanide SMMs: Borderline cases of purely 4f SMMs....37
   4.1. ZnYb SMMs....37
   4.2. ZnCe SMM....41
5. Heterobimetallic 4*f*4*f*' Lanthanide SMMs....43
6. Conclusion and perspectives....45

Edited Dec 26

Highlights

- Mononuclear Single Molecule Magnets (SMMs) containing Yb^{III}, Ce^{III}, Nd^{III}, Ho^{III} and Tm^{III} ions are reviewed.
- Polynuclear SMMs containing Yb^{III}, Ce^{III}, Nd^{III} and Ho^{III} are reviewed.
- Heterobimetallic $ZnYb^{III}/Ce^{III}$ and $4fYb^{III}$ SMMs are reviewed.
- Dynamic parameters and mechanisms of slow magnetic relaxation are deeply analysed.
- Magnetic properties and luminescence are correlated.

Abstract

Since the 1990s and the discovery of the first Single Molecule Magnets (SMMs), chemists and physicists have been working in concert to elaborate such molecular systems and understand their peculiar properties. Especially the use of lanthanide ions in the design of SMMs exploded with the discovery of the first example of mononuclear Tb^{III}-based complex which displayed a slow magnetic relaxation in 2003. This high-degree of interest comes from the diverse potential applications in quantum computing, high-density data storage devices and spintronics. Recently, the specific luminescence properties of the lanthanide ions were correlated to the magnetic ones. Even if the most common lanthanide ions used in the elaboration of SMMs are the Dy^{III}, Tb^{III} and Er^{III} ions, new SMMs involving others lanthanide ions (Yb^{III}, Ce^{III}, Nd^{III}, Ho^{III} and Tm^{III}) started to emerge. This review presents the research endeavour in the area of these uncommon lanthanide-based SMMs and underlines the different approaches to better understand their physical properties.

Keywords: Lanthanides, Design of Ligands, Luminescence, Single Molecule Magnets, energy splitting, relaxation processes

Edited Dec 26

Graphical abstract:

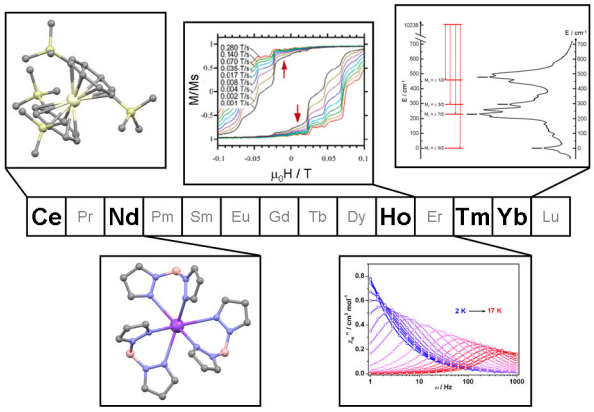

1. Introduction

Single-Molecule Magnets (SMMs) were discovered more than twenty years ago on a manganese-based polynuclear complex, the so-called Mn_{12} [1-3]. In this molecule the antiferromagnetic interactions between spins of Mn^{III} and Mn^{IV} ions stabilize a S=10 spin ground-state which can be trapped in up (M_s = +S) or down (M_s = -S) orientations. The magnetic memory is due to the energy barrier that blocks reversal of the magnetization. It is characterized by the slowing down of the magnetic relaxation. In 2003, Ishikawa *et al.* made a significant breakthrough with the discovery of SMM behaviour on mononuclear complexes based on lanthanide ions [4]. In this pioneering work, slow magnetic relaxation is observed for both Tb^{III} and Dy^{III} ions sandwiched between two phthalocyanine ligands (Double-decker phthalocyanine complexes). The magnetic properties for lanthanide SMMs is due to 4*f* electrons. On the one hand, those electrons are less exposed to ligand field effects than *d* electrons. On the other hand, spin-orbit coupling is larger for *f*-shell than for *d*-shell. Then the ligand field is considered as a perturbation of the spin-orbit coupling for *f*-block elements. For d-block elements, the spin-orbit coupling is partially, or even totally, quenched by the ligand field which minimize or suppress the magnetic anisotropy. For lanthanides the degeneracy of the ^{2S+1}L terms is removed by the spin-orbit coupling to produce $^{2S+1}L_J$. As a consequence, magnetic anisotropy is maximized in terms of amplitude for *f*-elements with respect to *d*-elements. The splitting of the $^{2S+1}L_J$ ground-state can be of the order of several hundreds of wavenumbers while it is only of a few tens of wavenumbers for first row transition metal ions [5]. The term symbols for the lanthanides of interest of this review is given in the Table 1.

Table 1. Term symbols for selected lanthanide ions.

Lanthanides	Ce^{III}	Nd^{III}	Ho^{III}	Tm^{III}	Yb^{III}
Ground term symbols	$^2F_{5/2}$	$^4I_{9/2}$	$^5I_8$	$^3H_6$	$^2F_{7/2}$

Mononuclear complexes of lanthanides contain formally all the ingredients to behave as SMM: large magnetic moments, magnetic anisotropy and a bistable ground state under the appropriate conditions. However, to trap the magnetic moment in two opposite directions the anisotropy needs to be axial (Ising type anisotropy). Long and Rinehart proposed five years ago an elegant survey to exploit the single ion anisotropy in the design of *f*-element SMMs [6]. Lanthanides are roughly decomposed in two families: those for which the electron distribution is oblate (expansion in a plane) and those for which the electron distribution is prolate (expansion along an axis). The most stable oxidation state for the whole lanthanide series is +III and in the following we will focus only on Ln^{III} complexes. La^{III} and Lu^{III} have a closed-shell electronic structure, they are magnetically silent and therefore set aside as far as magnetism is concerned. The ground-state of Eu^{III} is non magnetic ($^7F_0$) and the ground-state of Gd^{III} ($^8S_{7/2}$) has a spherical electronic distribution. Thus, those two ions can also be put aside as far as SMM behaviour is concerned. Pm^{III} is out of the race because of its radioactivity. We then focus on only ten elements of the lanthanide series. For an oblate distribution (Ce^{III}, Pr^{III}, Nd^{III}, Tb^{III}, Dy^{III} and Ho^{III}), negatively charged ligands must be disposed along an axis to stabilize the two Ising components $M_J=\pm J$ while they must be disposed within a plane for a prolate distribution (Sm^{III}, Er^{III}, Tm^{III} and Yb^{III}).

In the last ten years, hundreds of articles referring to lanthanide-based SMMs have been published [7-10] to analyse as well as to propose methods to enhance their magnetic properties [11-12]. In the vast majority, they focus on two ions, namely Dy^{III} and Tb^{III} [13]-[20]. Indeed, a rapid overview of the literature on lanthanide-based SMMs shows that more than 99% of the scientific production on this subject is related to Dy^{III}, Tb^{III} and Er^{III} based species, in mononuclear or polynuclear complexes, the most popular being Dy^{III}. In these complexes, those ions may be associated to transition metal ions or to other spin carriers such as organic radicals [21-23]. Two main reasons can be given for this quasi-monopoly: i) the large magnetic moments of such ions and ii) the relative facility to dispose the charges of the ligands above and below the flattened surfaces of the electronic distribution in the most popular octacoordinated coordination sphere

In this review, we set aside the Dy^{III}, Tb^{III} and Er^{III} based SMMs and only cover the work performed on SMMs with the less common tripositive lanthanide ions: Ce, Nd, Ho, Tm and finally, Yb. To date, no SMM behaviour has been observed on the two lanthanide ions Sm^{III} and Pr^{III}. We will focus at first on mononuclear SMMs based on Yb^{III}. This ion is certainly the most popular amongst the minority group. A specific attention will be devoted to quantitative analyses of the magnetic data to elucidate the relaxation processes involved as well as the mapping of the energy diagram in the ground-state multiplet. Then, the problematics of polynuclear Yb-based SMMs will be tackled in the frame of the presence or absence of interactions between magnetic centres. The third part of the review will be devoted to examples of SMMs based on Cerium, Neodymium, Holmium and Thulium. Finally, two specific sections will concern heterobimetallic Zn^{II}-4*f* complexes and heterometallic 4*f*-4*f'* complexes.

1. Mononuclear Ytterbium SMMs

This section describes firstly mononuclear Yb^{III}-based SMMs in which the lanthanide ion is surrounded solely by oxygen atoms. Then examples with different atoms in the Yb coordination sphere will be considered (Table 2).

Table 2. Mononuclear Ytterbium SMMs

Yb-SMM	Δ/cm^{-1}	τ_0/s	H/Oe	M_J ground state[e]	ref
$K_{13}[Yb(\mathbf{SiW_{11}O_{39}})_2]$ (**1**)	-	-	0	±5/2	[24]
$[Yb(\mathbf{H_3L^1})_2]Cl_3\cdot 5CH_3OH\cdot 2H_2O$ (**2**)	4.9[a]/156.9-187.9[d]	2.0×10^{-5}	400	±5/2+±1/2	[31]
$[Yb(tta)_3(\mathbf{L^2})]\cdot 2CH_2Cl_2$ (**3**)	4.2[a]/234[b]/234[d]	1.9×10^{-5}	1000	±5/2+±7/2	[45]
$[N(C_2H_5)_4]_3[Yb(\mathbf{L^3})_3]\cdot 2H_2O$ (**4**)	130[b]	/	1000	±5/2+±7/2	[49]
$Na[Yb\mathbf{L^4}(H_2O)]\cdot 4H_2O$ (**5**)	24.3[a]/197[d]	4.0×10^{-7}	1000	-	[50]
$[Yb(\mathbf{L^5})_3]\cdot 11H_2O$ (**6**)	11[a]/73[b]/20[c]	2.7×10^{-6}	2000	±5/2+±1/2	[51]
$[Yb(\mathbf{L^6})_2](NO_3)\cdot CH_3OH\cdot 0.5H_2O$ (**7**)	3.7[a]	1.0×10^{-5}	1000	-	[56]
$[Yb(\mathbf{L^6})(tta)_2]\cdot CH_3OH$ (**8**)	11.4[a]	1.8×10^{-7}	1000	-	[56]
$[Yb(\mathbf{L^7})]$ (**9**)	38[a]/464[b]/463.8[c]	1.5×10^{-8}	2000	-	[57]

[a] Effective energy barrier determined from ac measurements. [b] Effective energy barrier determined from luminescence measurements. [c] Effective energy barrier determined from dc measurements. [d] Effective energy barrier predicted by *ab initio* calculations. [e] When the ground state M_J value is not given is because it was not determined in the corresponding article.

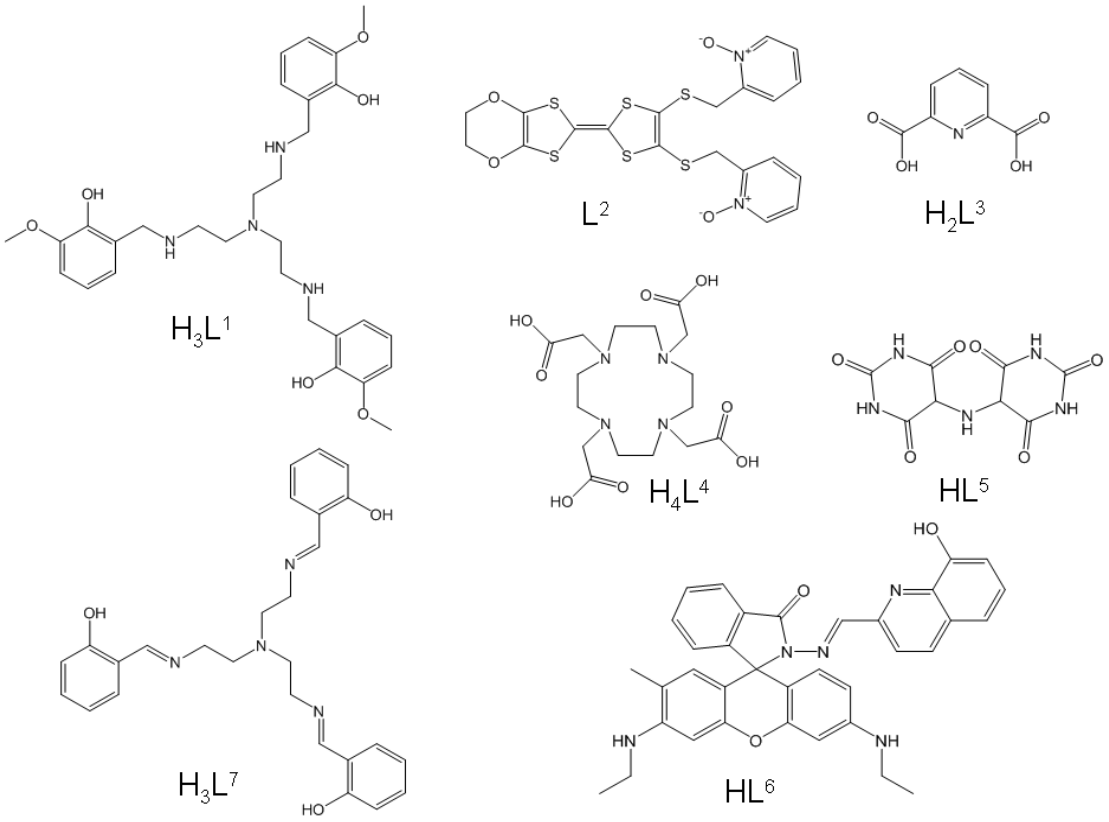

Scheme 1. Structures of selected ligands used to elaborate mononuclear Yb^{III} SMMs.

The first Yb^{III}-based SMM in which the lanthanide ion is surrounded by a fully oxygenated environment, was reported in 2009 by Coronado *et al.* [24] The $K_{13}[Yb(\mathbf{SiW_{11}O_{39}})_2]$ (**1**) was prepared using a previously reported method [25]. **1** is synthesized by mixing the incomplete $K_8[\beta_2\text{-}SiW_{11}O_{39}]\cdot 14H_2O$ polyoxometallate with hydrated $YbCl_3$ salt in acidic media. The X-ray structure revealed the encapsulation of the Yb^{III} ion by two $(\beta_2\text{-}SiW_{11}O_{39})^{8-}$ anionic units leading to a distorted square-antiprism coordination sphere (Figure 1).

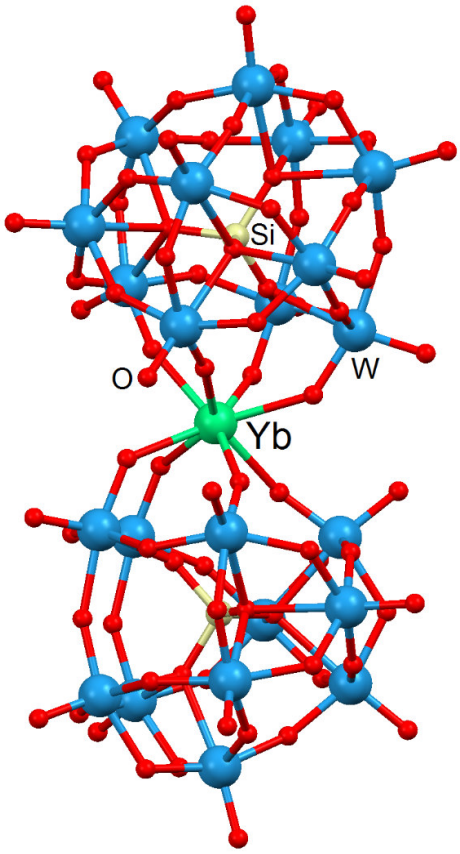

Figure 1. Molecular structure of $[Yb(\mathbf{SiW_{11}O_{39}})_2]^{13-}$. Potassium cations, water molecules of crystallization and hydrogen atoms are omitted for clarity. Adapted from ref [24].

The thermal variation of the magnetic susceptibility of **1** was evaluated using Ligand Field (LF) parameters. Taking into account a D_{4d} symmetry for the coordination sphere of Yb, the Hamiltonian was simplified as $\hat{H} = A_2^0 r^2 \alpha \hat{O}_2^0 + A_4^0 r^4 \alpha \hat{O}_4^0 + A_6^0 r^6 \alpha \hat{O}_6^0$ (where α, β, and γ coefficients are the constants tabulated by Stevens for each lanthanide [26], $\hat{O}_k^q$ are the operator equivalents and can be expressed as polynomials of the total angular momentum operators [27-28], r^k are radial factors, and A_k^q are numerical parameters). The ground-state corresponds to the M_J=±5/2 components of the $^2F_{7/2}$ multiplet with the first excited-state M_J=±7/2 localised at 100 cm^{-1}. Such ground-state allowed the observation of an out-of-phase component of the magnetic susceptibility below 10 K with both a maximum and a divergence in χ_M'' (where χ_M'' is the out-of-phase component of the magnetic susceptibility) due to the superparamagnetic blocking of the magnetic moments (thermally activated regime) and a fast tunnelling process (thermally independent regime), respectively. Unfortunately no quantitative dynamic parameters are given for this system. A quick comparison with the

phthalocyaninato complexes TBA[Ln(Pc)$_2$] (where Pc is the phthalocyanine) showed that the magnetic relaxation processes are faster in polyoxometallate due to a smaller separation between the lower-lying energy levels caused by the LF splitting. In other words, the nature of the first neighbouring atoms (oxygen *vs.* nitrogen) induces two different distortion of the D_{4d} coordination polyhedron (compressed *vs.* elongated).

In 2012, Tong *et al.* reported a surprising six-coordinated Yb^{III} complex based on the ligand tris(((2-hydroxy-3-methoxybenzyl)amino)ethyl)-amine (**H$_3$L^1**) (Scheme 1) which was produced by *in-situ* condensation and reduction of *o*-vanillin, tris(2-aminoethyl)amine and $NaBH_4$ [29-31]. In the resulting [Yb(**H$_3$L^1**)$_2$]Cl_3·5CH_3OH·2H_2O (**2**) compound (Figure 2a), the Yb^{III} ion adopts a distorted octahedral geometry which up to now remains the lowest coordination number for a purely Yb^{III}-based SMM. Nevertheless such geometry is not an obvious candidate for complementing the prolate nature of Yb^{III} ion.

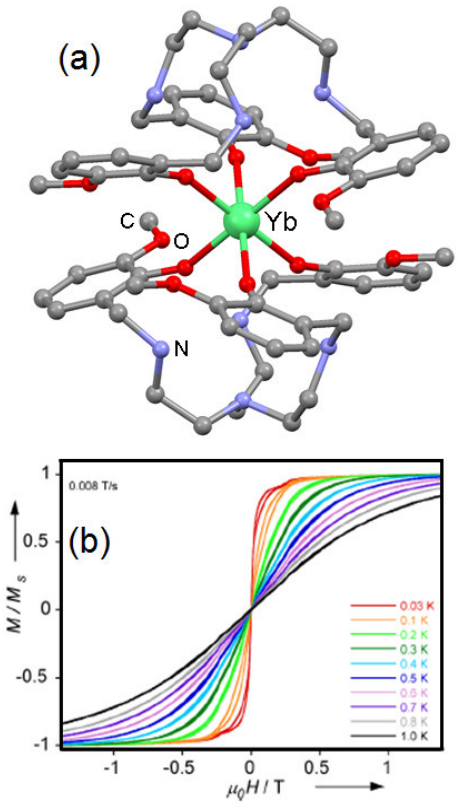

Figure 2. (a) Molecular structure of [Yb(**H$_3$L^1**)$_2$]$^{3+}$. Anions, solvent molecules of crystallization and hydrogen atoms have been omitted for clarity. (b) Normalized magnetization (M/M_s) *vs.* applied dc field (sweep rate of 0.008 T s^{-1}) in the temperature range 0.03-1.0 K applying the magnetic fields in the easy plane. Adapted from ref [31].

The symmetry of the coordination sphere is D_{3d}. Thus it has been proposed that the CF perturbations can be described with the effective Hamiltonian $\hat{H}_{CF} = B_0^2\hat{C}_0^2 + B_0^4\hat{C}_0^4 + B_3^4\hat{C}_3^4 + B_0^6\hat{C}_0^6 + B_3^6\hat{C}_3^6 + B_6^6\hat{C}_6^6$ [32]. The program CONDON [33] is used to fit the static magnetic susceptibility resulting in the doublet M_J=±5/2 as the main component of the ground-state with a non-negligible contribution of the M_J=±1/2 state (Table 2). In the absence of applied magnetic field, **2** does not behave as a SMM due to the quantum tunnelling of magnetization (QTM) which is allowed by the mixture of the M_J states in the ground-state. An optimal field of 400 Oe is enough to quench the QTM and permits one to observe a slow magnetic relaxation of the magnetization for **2** with an energy barrier of Δ=4.9 cm^{-1} and a pre-exponential factor τ_0=2.0×10^{-5} s. Attempts to determine the nature of the relaxation mechanism were done using the following spin-lattice relaxation time $\tau^{-1} = AT + BT^n + C\exp(-\Delta/kT)$ [34-39]. They found that the relaxation time obeys a $T^{-2.37}$ behaviour instead of an exponential temperature-dependence suggesting that the single-phonon direct process and optical acoustic Raman-like process are dominant. *Ab-initio* calculations have been performed on the molecular structure revealing that the ground Kramers doublet state is well separated from the first excited-state (from 156.9 to 187.9 cm^{-1} depending of the computational model) with strong transversal contributions for the Landé factor (g_x and g_y) in agreement with an easy plane like anisotropy [40]. The discrepancy between the energy barrier values extracted from the experimental ac measurements and the calculations gives more confidence in a direct process and excludes an Orbach process. Applying a magnetic field in the easy plane, a butterfly shaped hysteresis cycle was observed using a micro-SQUID magnetometer (Figure 2b) [41].

In the last few years, a new challenge appeared in the molecular magnetism community *i.e.* the addition of another physical property such as luminescence [42], chirality [43], ferroelectricity [44]… In this context, a remarkable system was elaborated starting from a redox-active tetrathiafulvalene-based ligand (**L^2**=4,5-ethylendioxy-4',5'-bis(2-pyridyl-N-oxidemethylthio)tetrathiafulvalene) (Scheme 1) and the metallo-precursor $Yb(tta)_3{\cdot}2H_2O$ (tta^-=2-thenoyltrifluoroacetonate anion). The resulting $[Yb(tta)_3(\mathbf{L^2})]{\cdot}2CH_2Cl_2$ (**3**) complex (Figure 3a) combines redox-activity, metal-centred luminescence and SMM behaviour [45]. The coordinated **L^2** ligand and the three tta^- anions confer a fully oxygenated surrounding for the Yb^{III} ion with a D_{4d} symmetry (the distortion was visualized by continuous shape measures performed with SHAPE 2.1 [46]). **L^2** can be reversibly oxidized twice at the potential of 0.42 and 0.87 V (V *vs.* SCE). This system crystallized in the triclinic P-1 space

group allowing the experimental determination of the magnetic anisotropy axis (Figure 3a). The experimental orientation of the anisotropy axis was compared with the calculated one, an approach still poorly developed, especially for Yb^{III}-based SMMs. Indeed, in the vast majority of studies, authors rely on the calculated magnetic anisotropy, which may lead to important misinterpretation [47]. In complex **3**, both orientations are in agreement with a difference of only 12°. The experimental (g_x=5.84, g_y=2.00 and g_z=1.77) and calculated values (g_x=5.96, g_y=0.73 and g_z=0.33) for the Landé factor are also in great agreement and illustrate an easy axial like anisotropy. Using this computational approach, the thermal magnetic susceptibility was reproduced with the doublet M_J=±5/2 ground-state (Table 2). The first excited doublet is found 234 cm^{-1} higher in energy.

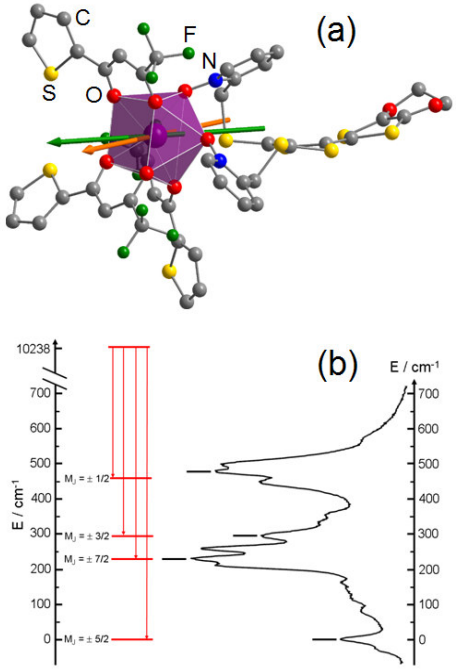

Figure 3. (a) Molecular structure of [Yb(tta)$_3$(**L^2**)] with experimental (orange) and theoretical (green) anisotropy axis. (b) The solid-state emission spectrum is given with an appropriate shift of energy scale. Correlation between the main contributions of the emission spectrum (black sticks) and the energy splitting of the $^2F_{7/2}$ multiplet ground-state obtained by MS-CASPT2/RASSI-SO calculations (red sticks). Adapted from ref [46].

Compound **3** does not show frequency dependence of the magnetic susceptibility without applied magnetic field while slow magnetic relaxation is observed with a dc field of 1000 Oe. An extended Debye model was used to extract the temperature dependence of the relaxation which can be treated in the frame of a thermally activated process with τ_0=1.9×10^{-5}

s and Δ=4.2 cm^{-1}. This energy barrier is much lower than the value determined from *ab-initio* calculations. The luminescence property of **3** was then studied in order to discriminate between the first two sets of data. Indeed, the luminescence spectrum can be viewed as a photography of the energy splitting of the $^2F_{7/2}$ multiplet ground-state. **3** displayed characteristic Yb^{III} luminescence upon irradiation in the Intra-Ligand Charge Transfer (ILCT) bands at 22200 cm^{-1} (Figure 3b). The experimental emission spectrum is characterized by more than the expected four contributions (corresponding to the degeneracy of the $^2F_{7/2}$ ground-state) and the additional emission contributions were attributed to transitions coming from the excited doublet states of the $^2F_{5/2}$ multiplet state (called "hot bands") [48]. Vibronic contributions were discarded by direct laser excitation of the f-f bands [49]. The luminescence spectrum gave the first excited doublet state localised at 234 cm^{-1} upon the ground-state, in perfect agreement with the computational results. The significant difference of energy barrier determined from the ac measurements with respect to luminescence and calculations seems to suggest that the Orbach process can be discarded in favour of a direct process as suggested for system **2**.

In the first examples, Yb neighbouring atoms consisted only of oxygen atoms but examples with a mixture of oxygen and nitrogen atoms have also been described. To the best of our knowledge, the first slow magnetic relaxation for an Yb^{III} complex was observed in 2006 by Ishikawa et al. [50]. In the complex $[N(C_2H_5)_4]_3[Yb(\mathbf{L}^3)_3]\cdot 2H_2O$ (**4**) (where $\mathbf{L}^3$= pyridine-2,6-dicarboxylate), the Yb^{III} ion is surrounded by six oxygen atoms and three nitrogen atoms coming from three dipicolinato anions (Figure 4).

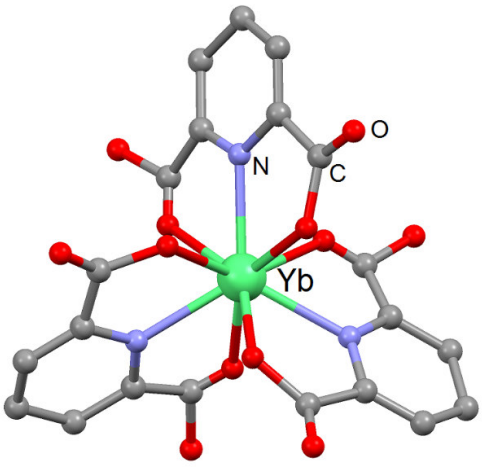

Figure 4. Molecular structure of $[Yb(\mathbf{L}^3)_3]^{3-}$. The tetraethylamonium cations and hydrogen atoms are omitted for clarity. Adapted from ref [50].

The out-of-phase signal of the magnetic susceptibility was detected in an applied magnetic field of 1000 Oe below 7 K. The LF interactions were evaluated using the Stevens method leading to the conclusion that the ground-state is mainly constituted by the doublet M_J=±5/2. The energy gap between the ground- and first excited-states was estimated to 130 cm^{-1} for **4** which is one order of magnitude higher than the energy gap found for the Er^{III} and Dy^{III} analogues. This important difference explains why the Yb^{III} analogue displayed slower relaxation of the magnetization.

One of the most popular and studied systems is undoubtedly the $Na[Yb\mathbf{L}^4(H_2O)]\cdot 4H_2O$ (**5**) where $\mathbf{L}^4$=1,4,7,10-tetraazacyclododecane-1,4,7,10-tetraacetic (scheme 1). In this mononuclear complex, the lanthanide is coordinated to four nitrogen atoms and four oxygen atoms and its surrounding can be described as a capped square antiprism [51]. The negative charges of the $\mathbf{L}^4$ ligand are almost contained in the equatorial plane of the complex (Figure 5a) and thus it is expected to have the easy anisotropy axis along the axial direction, *i.e.* along the Yb-O_{water} direction because of the prolate character of the Yb^{III} ion [6]. This prediction was confirmed by both experimental and computational determinations of the anisotropy axis (Figure 5b) which has been found respectively at 12° and 7° from the Yb-O_{water} direction. Thus, after vanishing of the fast relaxation by applying a magnetic field of 1000 Oe, compound **5** behaves as a SMM with dynamic parameters of $\tau_0=4.0\times10^{-7}$ s and Δ=24.3 cm^{-1} (Table 2).

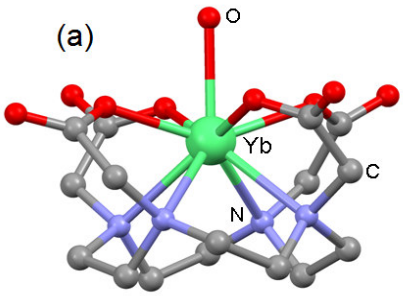

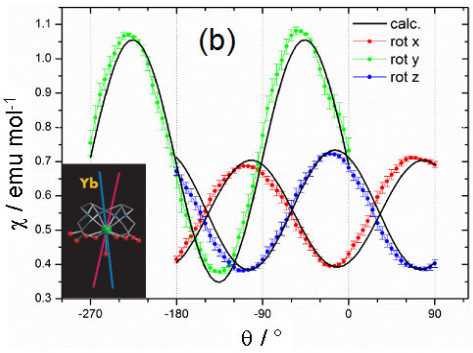

Figure 5. (a) Molecular structure of $[Yb\mathbf{L}^4(H_2O)]^-$. Water molecules of crystallization, hydrogen atoms and sodium cations are omitted for clarity. (b) Experimental and computational magnetization contributions. In inset, experimental (pink) and calculated (blue) magnetization easy axis at 2 K. Adapted from ref [51].

Ab-initio calculations performed on this system gave an energy barrier of 197 cm^{-1} which is much higher than the value determined from the ac measurements probably due to transverse components of the crystal field which allow efficient under-barrier mechanisms of relaxation. Finally, based on the results obtained for the whole series of $Na[Ln\mathbf{L}^4(H_2O)]\cdot 4H_2O$ compounds, Boulon *et al.* proposed that the orientation of the easy magnetization is driven by the correlation between the prolate/oblate electronic density distribution of the *4f* ion and the ligand geometry even if the presence of a coordinated water molecule is enough to drastically change this orientation [51].

The mononuclear complex $[Yb(\mathbf{L}^5)_3]\cdot 11H_2O$ (**6**) is obtained from the mixing of two aqueous solutions of murexide and nitrate salt of Yb^{III} [52]. This compound can be seen as an analogue of **4** since the three murexide ligands confer a N_3O_6 environment to the metallic centre (Figure 6a). Nevertheless, Guillou and collaborators went a step forward in the analysis of the physical properties. Firstly, even if a SHAPE analysis led to a C_{4v} spherical-capped square-antiprism as the best description of the coordination environment, **6** was better described with a D_{3h} symmetry on the basis of point charges. In fact the main negative charges come from the oxygen atoms that are closer to the Yb^{III} ion than the nitrogen atoms. This description is supported by Stevens operators, which can perfectly reproduce the magnetic susceptibility if they are taken for a D_{3h} symmetry ($\hat{H} = B_2^0\hat{O}_2^0 + B_4^0\hat{O}_4^0 + B_6^0\hat{O}_6^0 + B_6^6\hat{O}_6^6$) but not for a C_{4v} symmetry.

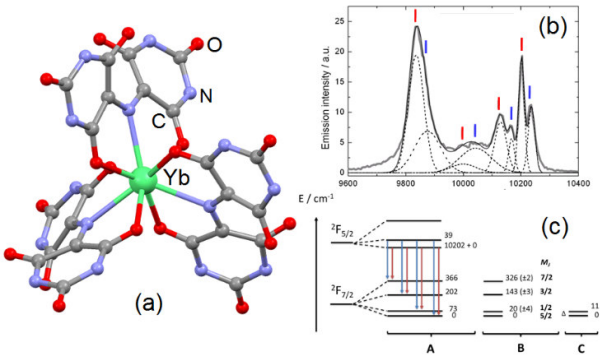

Figure 6. (a) Molecular structure of $[Yb(\mathbf{L}^5)_3]$. Water molecules of crystallization and hydrogen atoms are omitted for clarity. (b) Solid-state luminescence spectrum of **6** at 77 K

under an irradiation of 25000 cm^{-1}. Blue and red sticks are components coming from the lowest-energy and first excited M_J states of the $^2F_{5/2}$ multiplet state. (c) Extracted energy diagram from luminescence spectrum (A), from dc measurements (B) and ac measurements (C). Adapted from ref [52].

Considering this D_{3h} symmetry for the surrounding, the M_J=±5/2 doublet is the main component of the ground-state while the first excited-state lies at 20 cm^{-1} (Table 2). A second set of data for the energy splitting was obtained by the dynamic magnetic properties. Applying the optimal magnetic field of 2000 Oe permits to highlight the SMM behaviour of **6** with a thermally activated regime characterized by an energy barrier of 11 cm^{-1} and a relaxation time of $\tau_0=2.7\times10^{-6}$ s (Table 2). The last set of data could be obtained from the photophysical properties. The murexide ligand shows a dark red colour coming from intense absorption bands. These intense absorption bands have been used by to irradiate compound **6** and guaranteed an efficient sensitization of the Yb^{III} ion. Thus eight components are identified in the luminescence spectrum (Figure 6b) which is more than the expected splitting of the $^2F_{7/2}$ ground multiplet state. Since the same energy difference remains between two consecutive transitions, the four additional emissive lines were attributed to the contribution of the first excited M_J state of the $^2F_{5/2}$ multiplet state (Figure 6c). The maximum splitting of the ground-state is 366 cm^{-1} in agreement with high symmetry complexes like helicate (372 cm^{-1}) [53] and trisdipicolinate (348 cm^{-1}) [54] enforcing the analogy with compound **4**.

The more common number of coordination for the Yb^{III} ion is eight even if the three previous examples **4**-**6** showed a nine-coordination environment. The rhodamine-6G-2-(hydrozinomethyl) quinolin-8-ol ligand (**L**^{6}) was used by C. Duan and coll. to sensitise the Yb^{III} near-infrared luminescence and to build SMMs [55]. W. Huang *et al.* played with the strength of the chelating character of the anions coordinated to the Yb^{III} ion in the starting salt to change the ratio between the metal and **L**^{6}. Thus the weak chelating nitrate led to the formation of the 1:2 $[Yb(\mathbf{L}^6)_2](NO_3)\cdot CH_3OH\cdot 0.5H_2O$ (**7**) complex (Figure 7a) while the strong chelating tta^- led to the formation of the 1:1 $[Yb(\mathbf{L}^6)(tta)_2]\cdot CH_3OH$ (**8**) complex (Figure 7b) [56]. The X-ray structures of these samples revealed O_4N_4 and O_6N_2 environments for **7** and **8**, respectively. Despite the different environments, both compounds display a SMM behaviour under an applied field of 1000 Oe (Figure 7) with energy barriers of 3.7 and 11.4 cm^{-1} (Table 2).

Edited Dec 26

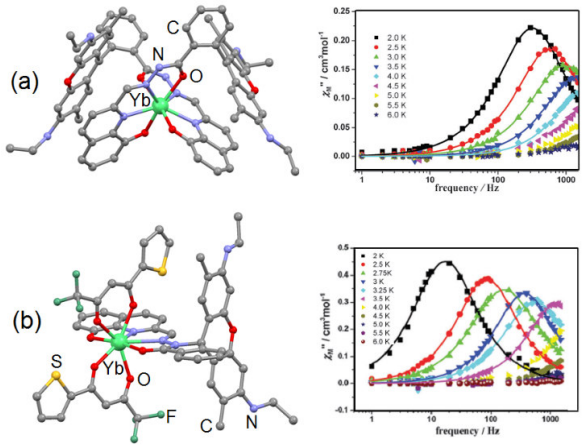

Figure 7. X-ray structures and frequency dependence of the magnetic susceptibility measured in a 2-6 K temperature range for $[Yb(\mathbf{L^6})_2]^+$ (a) and $[Yb(\mathbf{L^6})(tta)_2]$ (b). Adapted from ref [56].

Yb-based SMMs allow one to extract the energy splitting of the multiplet ground-state by several methods *i.e.* Stevens operator (dc data), ac data, *ab-initio* calculations and luminescence spectrum. In this context, the later approach often displays more than the expected number of emissive lines for the $^2F_{7/2}$ multiplicity due to possible participation of excited doublets of the excited $^2F_{5/2}$ multiplet state. In contrary, absorption is an adequate spectroscopy to take a clear picture of the energy splitting of the multiplet excited-state. Such demonstration was done by K. S. Pedersen *et al.* for the $[Yb(\mathbf{L^7})]$ (**9**) compound [57] (where $\mathbf{L^7}$=2,2',2''-tris(salicylideneimino)triethylamine [58]). This derivative is one of the compounds of the series recently studied by Riley, Sorace, Dreiser, Sessoli *et al.* [59-62]. The X-ray structure of **9** revealed an Yb^{III} ion in a N_4O_3 seven-coordination environment (Figure 8a). A complete energy splitting of both the $^2F_{7/2}$ multiplet ground-state and $^2F_{5/2}$ multiplet excited-state was established combining emission (at 5 K) and absorption (at 10 K) studies (Figure 8b). An energy barrier value of 464 cm^{-1} was extracted from the spectroscopic measurements. Since **9** crystallizes in the P3c1 space group (trigonal symmetry), eight independent ligand field parameters are enough to describe the electronic energy spectrum. Static (dc) magnetization data of both single crystal and polycrystalline sample of **9** have been reproduced considering an energy splitting of 463.8 cm^{-1} between the ground-state and first excited doublet.

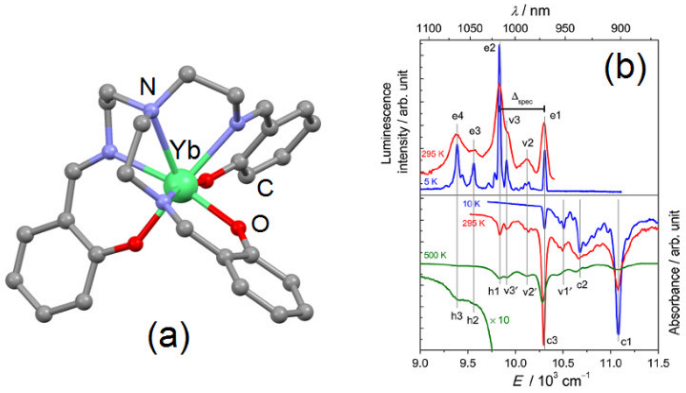

Figure 8. (a) X-ray structure of **9**. Hydrogen atoms are omitted for clarity. (b) NIR absorption (bottom) and luminescence (above) of **9**. c, h, e and v denote cold absorption, hot absorption, emission, and vibrational transitions, respectively. Adapted from ref [57].

Then in order to determine the anisotropy of the system, they doped the Eu^{III} analogue with 5 % of **9** and studied by X-band EPR a resulting single crystal. The relevant g factors are $g_{//}$=4.29 and $g_{\perp}$=2.90. The easy axial character of the magnetic anisotropy of **9** drives the authors to perform the ac measurements. They revealed a field-induced SMM behaviour with Δ=38 cm^{-1} and τ_0=1.5×10^{-8} s (Table 2). Thus, there is a clear discrepancy between the energy gap determined using an Orbach model and the value determined from the absorption and luminescence spectra (Figure 8b). In case of polycrystalline sample, fitting of the complete-range data for the temperature-dependence of the relaxation time with the following expression: $\tau^{-1} = CT^n + DT^m$ afforded C= 0.15 s^{-1} $K^{-6.2}$ (high temperature) and D= 258 s^{-1} K^{-1} (low temperature) in agreement with what is expected for an alternative Raman relaxation mechanism [35] (high temperature) and a normal direct process [27] (low temperature). In conclusion, the relaxation of the magnetization of **9** is governed by Raman, direct and QTM processes while the Orbach relaxation mechanism can be excluded of the description of the magnetization dynamics.

2. Polynuclear Ytterbium SMMs

As seen in the previous section, the number of mononuclear SMMs based on Yb^{III} ion is quite limited compared to what is observed for the most used lanthanide ions such as Tb^{III}, Dy^{III} and Er^{III}. Nevertheless, in the last years, several examples of dinuclear complexes as well as mono-dimensional species which display SMM behaviour have been published. These examples are mainly elaborated from TTF-based ligands and Schiff base ligands (Scheme 2).

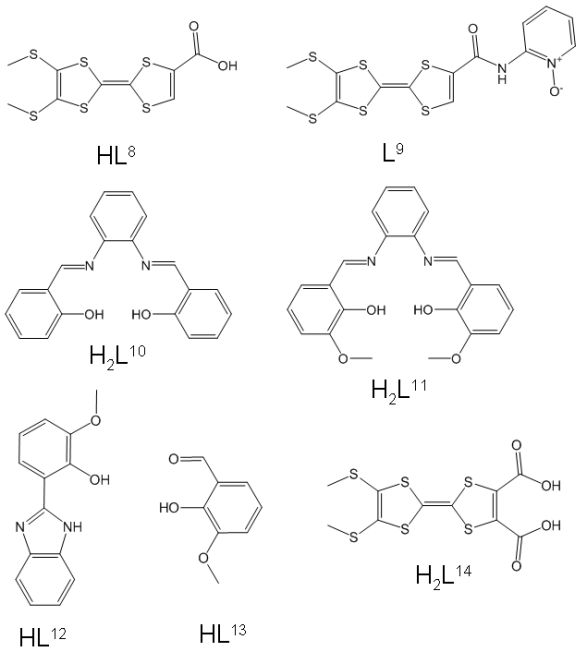

Scheme 2. Structures of selected ligands used to elaborate the polynuclear Yb^{III} SMMs.

The increase of nuclearity might introduce a new parameter to take into account in the interpretation of the magnetic properties, *i.e.* the intra-molecular magnetic interactions (dipolar and/or exchange). The next section reviews all polynuclear Yb^{III}-based SMMs published to date. They are listed in Table 3.

Table 3. Polynuclear Ytterbium SMMs

Yb-SMM	Δ/cm^{-1}	τ_0/s	H/Oe	M_J Ground-state[d]	ref
$[Yb(tta)_2(\mathbf{L^8})(\mathbf{L^9})]_2 \cdot 1.4CH_2Cl_2$ (**10**)	14.7[a]/16[b]/2.6[c]	1.5×10^{-8}	0-2000	±7/2	[63]
$[Yb_2(\mathbf{L^{10}})_2(acac)_2(H_2O)] \cdot 2CH_2Cl_2$ (**11**)	17[a]	6.8×10^{-7}	1600	-	[64]
$[Yb_2(\mathbf{L^{11}})_3(CH_3OH)] \cdot 3CH_3CN$ (**12**)	10.1[a]	1.6×10^{-6}	3000	-	[65]
$[Yb_2(\mathbf{L^{11}})(\mathbf{L^{12}})(\mathbf{L^{13}})(CH_3OH)(H_2O)_2](ClO_4)_2$ (**13**)	1.4[a]	3.7×10^{-5}	3000	-	[65]
$[Yb_2(\mathbf{L^{11}})(OAc)_4(CH_3OH)_2] \cdot 2CH_3OH$ (**14**)	6.6[a]	4.8×10^{-6}	3000	-	[65]
$\{[Yb_2(\mathbf{L^{11}})(OAc)_4] \cdot 3H_2O\}_n$ (**15**)	1.7[a]	1.0×10^{-5}	3000	-	[65]
$\{[Yb(\mathbf{L^{14}})(H_2O)_3(DMF)](\mathbf{HL^{14}}) \cdot H_2O\}_n$ (**16**)	19.5[a]	1.0×10^{-7}	1000	-	[66]

[a] Effective energy barrier determined from ac measurements. [b] Effective energy barrier determined from luminescence measurements. [c] Effective energy barrier determined from dc measurements. [d] When the ground state M_J value is not given is because it was not determined in the corresponding article.

The first dinuclear complex is a multi-properties SMM elaborated by the mixture in a 1:1:1 ratio of the metallo-precursor $Yb(tta)_3{\cdot}2H_2O$ with the two $\mathbf{L^8}$ (4,5-bis(thiomethyl)-4'-carboxylate-tetrathiafulvalene) and $\mathbf{L^9}$ (4,5-bis(thiomethyl)-4'-ortho-pyridyl-N-oxide-carbamoyltetrathiafulvalene) ligands [63]. The obtained centro-symmetric dinuclear complex $[Yb(tta)_2(\mathbf{L^8})(\mathbf{L^9})]_2{\cdot}1.4CH_2Cl_2$ (**10**) contains two Yb^{III} ions in a O_8 distorted dodecahedral coordination surrounding (D_{2d} symmetry). Both Yb^{III} ions are bridged by the N-O functions of the $\mathbf{L^9}$ ligands (Figure 9a).

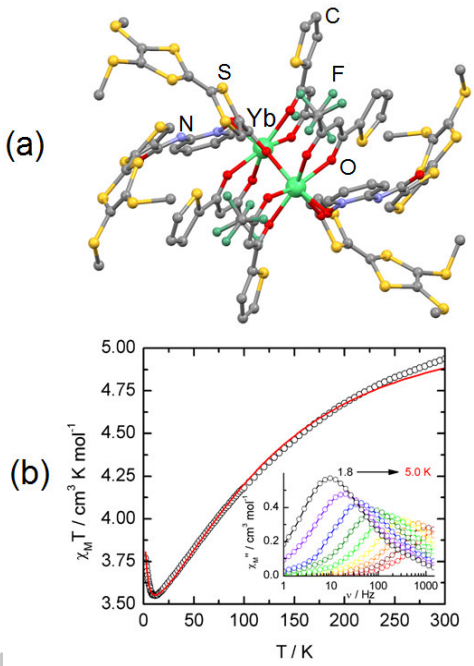

Figure 9. (a) Molecular structure of $[Yb(tta)_2(\mathbf{L^8})(\mathbf{L^9})]_2$. Dichloromethane molecules of crystallization and hydrogen atoms are omitted for clarity. (b) Temperature dependence of the $\chi_M T$ product (open circles) with the best-fitted curve (red line). The inset shows the frequency dependence of the out-of-phase component of χ_M measured with an external field of 2000 Oe. Adapted from ref [63].

Attempts to reproduce the static magnetic properties were done using an extended Stevens operators technique taking into account both crystal field effects and possible ferromagnetic interactions (because of the increase of $\chi_M T$ *vs*. T curve below 9 K (Figure 9b)). The Hamiltonian which was considered in the D_{2d} symmetry environment is the following:

$$\hat{H} = \sum_{i=1}^{2}\left(B_2^0\hat{O}_{2i}^0 + B_4^0\hat{O}_{4i}^0 + B_6^0\hat{O}_{6i}^0 + B_4^4\hat{O}_{4i}^4 + B_6^4\hat{O}_{6i}^4\right) + \beta g_J\left(\hat{J}_1 + \hat{J}_2\right)\cdot\vec{H} - J\ \hat{J}_1\cdot\hat{J}_2 .$$

In this expression, the first part corresponds to the crystal field at the two Yb^{III} ions while the second part corresponds to the Zeeman effect on the lanthanide magnetic moment coupled through *J*. It was possible to fit the magnetic susceptibility without interaction (*J*=0) and in the approximation of the Yb^{III} in a higher D_{4d} symmetry. The ground-state under these conditions is given by pure $M_J = \pm 7/2$ states with the first excited-states ($M_J = \pm 1/2$) lying only 2.57 cm^{-1} above. The increase of the $\chi_M T$ product at low temperature was explained by the thermal depopulation of the $M_J = \pm 1/2$ (lowest value for a $^2F_{7/2}$ multiplet state) which is localised a few cm^{-1} above the $M_J = \pm 7/2$ ground states (highest value for a $^2F_{7/2}$ multiplet state). The stabilisation of the $M_J = \pm 7/2$ states could find its origin in the strong equatorial coordination of the carboxylate ligands in agreement with the prolate electron density proposed by Long and co-workers [6]. The stabilisation of such high M_J state led to the observation of a SMM behaviour without applied magnetic field. The observation of an out-of-phase signal without applied magnetic field for such compounds was previously described only for complex **1** [24]. Nevertheless the extraction of quantitative dynamic parameters required the shift of the χ_M" to lower frequencies by application of an external field of 2000 Oe (Inset of Figure 9b). Under these conditions the energy barrier was 14.7 cm^{-1} (Table 3). Irradiation of the Ligand-to-Ligand Charge Transfer (LLCT) from 15380 to 22200 cm^{-1} allowed the sensitization of the Yb^{III}-centred luminescence which gave a third value of the energy separation between the ground- and first excited-states (16 cm^{-1}) (Table 3). A fairly good correlation was obtained between the crystal field splitting extracted from the static and dynamic magnetic measurements and the luminescence. The underestimated energy barrier extracted from ac measurements was attributed to the simple model used or/and to direct process involved in the relaxation of the magnetization.

A second example of dinuclear SMM of Yb^{III} ion is obtained using a salen type ligand ($H_2\mathbf{L^{10}}$=N,N'-bis(salicylidene)-o-phenylenediamine) and the $Yb(acac)_3$ metallo-precursor ($acac^-$=acetylacetonate anion) [64]. The two Yb^{III} ions in the compound of formula $[Yb_2(\mathbf{L^{10}})_2(acac)_2(H_2O)]\cdot 2CH_2Cl_2$ (**11**) are bridged through the phenoxide groups (Figure 10). As for compound **10**, the increase of the $\chi_M T$ product at low temperature seems to signify that weak ferromagnetic interactions are taking place between the two metals. **11** behaves as a SMM in an applied magnetic field of 1600 Oe with Δ=17 cm^{-1} and $\tau_0 = 6.8\times10^{-7}$ s (Table 3). *Ab-initio* calculations at the CASSCF level have been performed for this system highlighting the magnetic difference between the two Yb^{III} ions. In particular, the two anisotropy axes have been found not parallel. The absence of SMM behaviour without external field was

attributed to the significant transversal g factors and the large tunnelling gap in the ground exchange doublet (0.01 cm^{-1}) allowing a strong quantum tunnelling of the magnetization.

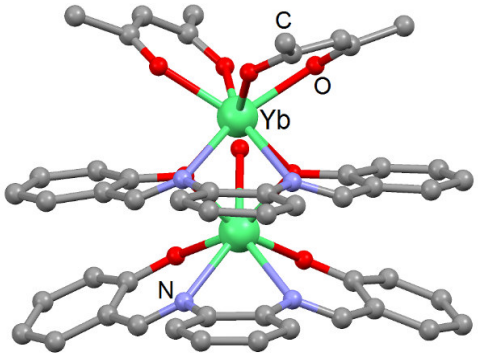

Figure 10. Molecular structure of $[Yb_2(\mathbf{L}^{10})_2(acac)_2(H_2O)]$. Dichloromethane molecules of crystallization and hydrogen atoms are omitted for clarity. Adapted from ref [64].

G.-M. Li and co-workers confirmed that the association of Yb^{III} ions and salen-type ligands is efficient to obtain field-induced SMMs [65]. They synthesized three dinuclear complexes and a one-dimensional compound using the N,N'-bis(2-oxy-3-methoxybenzylidene)-1,2-phenylenediamine ligand ($H_2\mathbf{L}^{11}$) and diverse ytterbium salts. In the three samples $[Yb_2(\mathbf{L}^{11})_3(CH_3OH)]\cdot 3CH_3CN$ (**12**), $[Yb_2(\mathbf{L}^{11})(OAc)_4(CH_3OH)_2]\cdot 2CH_3OH$ (**14**), and $\{[Yb_2(\mathbf{L}^{11})(OAc)_4]\cdot 3H_2O\}_n$ (**15**), two crystallographically independent Yb^{III} ions are identified respectively in D_{4d} (for Yb1) and C_{2v} (for Yb2) symmetries. Nevertheless, the nature of the environment is different: N_2O_6 and N_4O_4 for **12**, O_8 and N_2O_6 for both **14** and **15** (Figure 11). The compound $[Yb_2(\mathbf{L}^{11})(\mathbf{L}^{12})(\mathbf{L}^{13})(CH_3OH)(H_2O)_2](ClO_4)_2$ (**13**) revealed two crystallographically independent Yb^{III} ions in D_{3h} (O_9 environment) and C_{2v} (N_2O_6 environment) symmetries (Figure 11b). The four compounds **12**-**15** displayed a slow magnetic relaxation in an applied magnetic field of 3000 Oe with energy barrier ranging from 1.4-10.1 cm^{-1} and relaxation time ranging from 1.0×10^{-5} to 1.6×10^{-6} s (Table 3). The four compounds showed NIR luminescence from the Yb^{III} ion as confirmed by both lifetime and quantum yield. Unfortunately, no attempt of correlation between optical and magnetic properties has been realised. Even if the nature of both environments as well as ligands are not the same among the complexes, the energy barrier values were correlated to structural characteristics for **12**, **14** and **15** in which the symmetry of the Yb coordination spheres is the same. G.-M. Li and co-workers concluded that larger the dihedral angle between the two triangle planes are, longer the distances between the two Yb^{III} ions are and higher are the energy barriers.

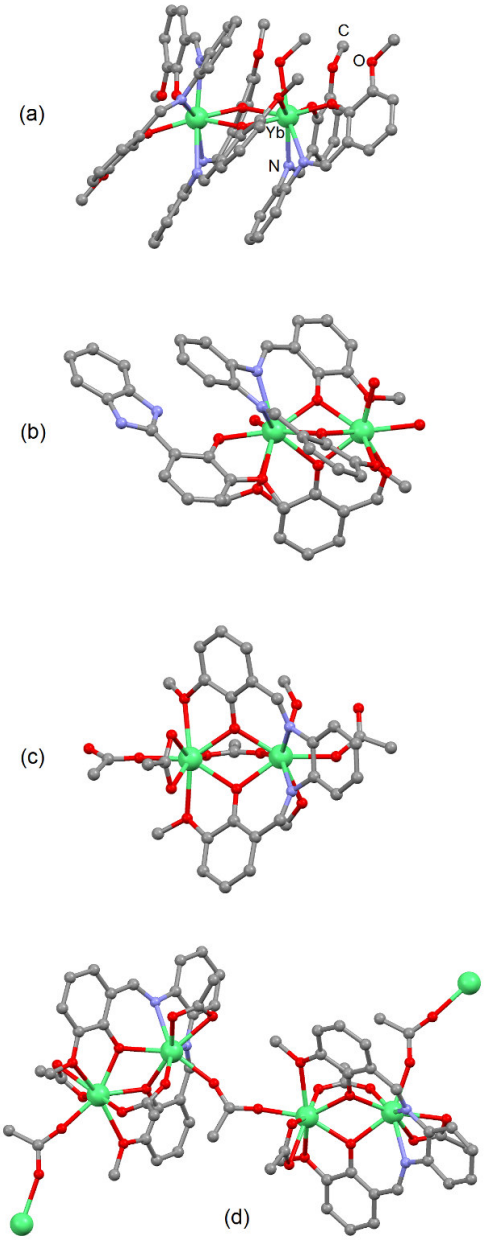

Figure 11. Molecular structures of $[Yb_2(\mathbf{L}^{11})_3(CH_3OH)]$ (a), $[Yb_2(\mathbf{L}^{11})(\mathbf{L}^{12})(\mathbf{L}^{13})(CH_3OH)(H_2O)_2]^{2+}$ (b), $[Yb_2(\mathbf{L}^{11})(OAc)_4(CH_3OH)_2]$ (c) and **15** (d). Solvent molecules of crystallization and hydrogen atoms are omitted for clarity. Adapted from ref [65].

The compound **15** was the first Yb-based mono-dimensional assembly of SMM which consequently displayed slow magnetic relaxation. One year later, Pointillart *et al.* published the first redox-active chain of Yb^{III} which shows similar behaviour [66]. This polymer of

formula $\{[Yb(\mathbf{L}^{14})(H_2O)_3(DMF)](\mathbf{HL}^{14})\cdot H_2O\}_n$ (**16**) ($\mathbf{L}^{14}$=4,5-bis(carboxylate)-4',5'-methyldithiotetrathiafulvalene) (Scheme 2) was obtained by mixing the $Yb(hfac)_3\cdot 2H_2O$ metallo-precursor with the disodium salt of $\mathbf{L}^{14}$ in dimethylformamide. Any $hfac^-$ ancillary ligand was found in the crystallographic structure due to the exchange with the coordinated anionic $\mathbf{L}^{14}$ ligands. The Yb^{III} ions are bridged through the carboxylate functions of $\mathbf{L}^{14}$ in a $\mu_2(\eta_1,\eta_1)$ mode (Figure 12a) leading to the formation of a cationic monodimensional polymer. The Yb^{III} ion adopts a distorted square antiprism (D_{4d} symmetry) as coordination sphere. The neutrality of the sample is assumed by free mono-protonated $H\mathbf{L}^{14}$.

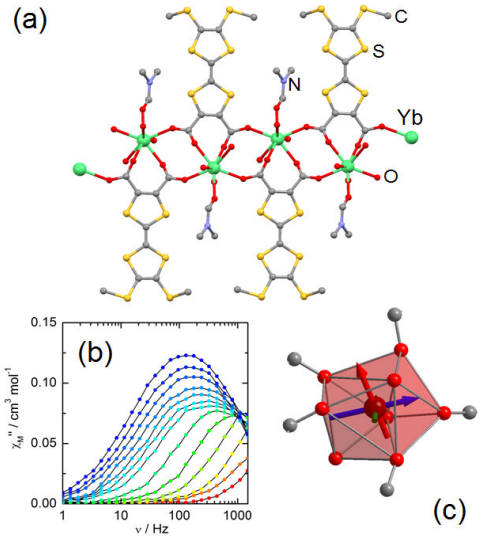

Figure 12. (a) Molecular structure of $\{[Yb(\mathbf{L}^{14})(H_2O)_3(DMF)](\mathbf{HL}^{14})\}_n$. Anionic $H\mathbf{L}^{14}$, water molecules of crystallization and hydrogen atoms are omitted for clarity. (b) Frequency dependence of the out-of-phase component of the ac susceptibility measured between 1.8 and 6 K in an external dc field of 1000Oe. (c) D_{4d} square antiprism polyhedron with the principal magnetic axes (g_x: blue, g_y: green, g_z: red) of **16**. Adapted from ref [66].

As for almost all Yb^{III}-based SMMs, no out-of-phase signal of the magnetic susceptibility is observed without applied magnetic field, whereas an optimal field of 1000 Oe led to a frequency dependence of the magnetic susceptibility (Figure 12b). The temperature dependence of the relaxation time was reproduced with two Arrhenius profiles. Above 3K, the extracted energy barrier of 19.5 K is one of the highest for Yb-based SMM while the relaxation time of 1.0×10^{-7} s is classical for such systems. Experimental single-crystal rotating magnetometry were performed to determine the Landé factors along the three directions. The

results were surprising since the anisotropy was found more planar than axial with g_x=3.24, g_y=1.53 and g_z=4.25 due to the peculiar environment around the Yb^{III} ion.

In this section, an exhaustive list of Yb^{III}-based SMMs was reviewed with the description of either mono-, di-nuclear or one-dimensional compounds. Surprisingly no high nuclearity SMM involving Yb^{III} ions has been reported to date. Nevertheless the nature of the coordination sphere is varied with different nitrogen/oxygen ratios leading to both easy uniaxial and easy planar anisotropies. In these examples, the slow magnetic relaxation takes place through direct, Raman and quantum processes while the classical two phonon Orbach process has been discarded. Finally, the NIR luminescence of the Yb^{III} ion is a key tool to increase the level of understanding of the magnetic properties.

3. SMMs built from other uncommon lanthanide ions

3.1. Cerium SMMs

The Ce^{III} ion possesses only one single electron in its *4f* shell. Nevertheless the spin-orbit coupling is strong enough to create significant magnetic anisotropy and then an energy barrier between the two orientations of the magnetization. The possibility to elaborate SMMs from Ce^{III} was thus demonstrated in two recent publications [67,68].

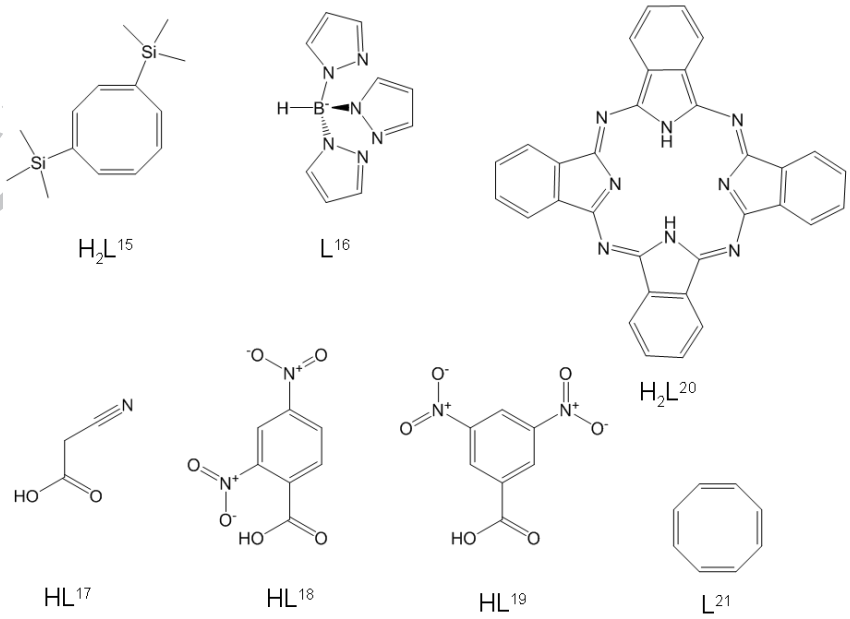

Scheme 3. Structures of selected ligands used to elaborate Ce^{III}, Nd^{III}, Ho^{III} and Tm^{III} SMMs.

Table 4. Lanthanide SMMs (Ln=Ce^{III}, Nd^{III}, Ho^{III} and Tm^{III}).

Ln-SMM	Δ/cm^{-1}	τ_0/s	H/Oe	M_J ground state[e]	ref
$Li(DME)_3[Ce(\mathbf{L^{15}})_2]$ (**17**)	20.9[a]/503[d]	1.2×10^{-6}	400	±1/2	[67]
$Li(DME)_3[Nd(\mathbf{L^{15}})_2]$ (**18**)	14.6[a]	5.5×10^{-5}	1000	-	[74]
(**19**)*	24.4[a]/4.4[a]	2.6×10^{-7}/2.1×10^{-5}	200	-	[68]
	9.1[a]	1.1×10^{-6}	1400		
$[Nd(\mathbf{L^{16}})_3]$ (**20**)	2.8[a]/119[b]/115[c]	4.2×10^{-5}	100	±5/2+±7/2-	[76]
$\{[Nd_2(\mathbf{L^{17}})_6(H_2O)_4]\cdot2H_2O\}_n$ (**21**)	18.5[a]/72.3[d]	1.75×10^{-7}	1500	-	[88]
$\{[Nd(\mathbf{L^{18}})_3(H_2O)_2]\cdot2CH_3CN\}_n$ (**22**)	19[a]/77.8[d]	4.1×10^{-7}	2000	-	[94]
$\{[Nd(\mathbf{L^{19}})_2(CH_3COO)(H_2O)_2]\}_n$ (**23**)	20[a]/87.3[d]	3.1×10^{-7}	3500	-	[94]
$TBA[Ho(\mathbf{L^{20}})_2]$ (**24**)	15[c]	-	-	±5	[96]
$Na_{13}[Ho(\mathbf{SiW_{11}O_{39}})_2]$ (**25**)	6[c]	-	0	±4	[24]
$Na_9[Ho(\mathbf{W_5O_{18}})_2]$ (**26**)	16[c]	-	0	±4	[101]
$[Ho_5O(OiPr)_{13}]$ (**27**)	278[a]	1.5×10^{-9}	5500	-	[102]
$K_{12}[Ho(H_2O)P_5W_{30}O_{110}]\cdot nH_2O$ (**28**)	0.6[a]/14[c]	6.0×10^{-3}	0	±8	[103]
$[(Tp)Tm(\mathbf{L^{21}})]$ (**29**)	90.4[a]	4.7×10^{-7}	2000	±6	[116]
$[(Tp^*)Tm(\mathbf{L^{21}})]$ (**30**)	46[a]	2.4×10^{-6}	2000	±6	[116]

[a] Effective energy barrier determined from ac measurements. [b] Effective energy barrier determined from luminescence measurements. [c] Effective energy barrier determined from dc measurements. [d] Effective energy barrier predicted by *ab initio* calculations. [e] When the ground state M_J value is not given is because it was not determined in the corresponding article. * (**19**)=$[Ce(DMSO)_8][Ce(NO_3)_2(DMSO)_4(\mathbf{Mo_8O_{26}})_{0.5}][Mo_6O_{19}]$

The first example of pure Ce^{III} based-SMM was published in 2014 by M. Murugesu *et al.* [67]. The complex $Li(DME)_3[Ce(\mathbf{L^{15}})_2]$ (**17**) was synthesised following a reported method for the Dy^{III} analogue [69] *i.e.* reacting $CeCl_3$ salt with the 1,4-bis(trimethylsilyl)-cyclooctatetraenyl dianion ($\mathbf{L^{15}}$) in a 3:2 molar ratio. The planar $\mathbf{L^{15}}$ ligand was used to provide an axial symmetry (C_8 axis) with a strictly axial coordination environment around the Ce^{III} ion. This choice was driven by the prediction of Rinehart *et al.* who argued that such symmetry would be ideal to maximize the axial anisotropy of Ce^{III} ions [6].

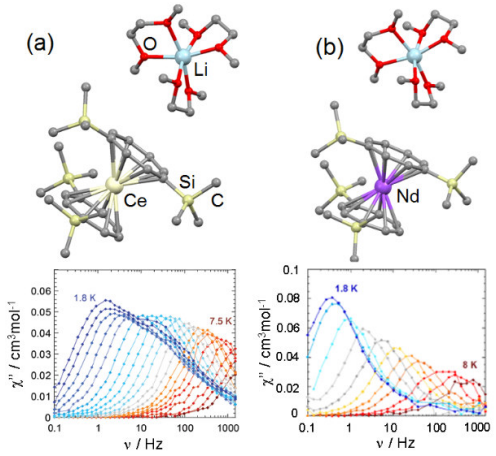

Figure 13. (Top) Molecular structures of $Li(DME)_3[Ln(\mathbf{L^{15}})_2]$ ($Ln=Ce^{III}$ (**17**) (a) and Nd^{III} (**18**) (b)). (Bottom) Frequency dependence of the magnetic susceptibility for (**17**) (a) and (**18**) (b) measured in a 1.8-8 K temperature range. Adapted from ref [67] and [74].

The dynamic magnetic properties of **17** revealed no frequency dependence of the magnetic susceptibility without applied magnetic field, while a small applied field (400 Oe) is enough to observe strong frequency dependence (Figure 13a). Above 3.5 K, a single relaxation time is measured (1.2×10^{-6} s), and the SMM was characterised with an energy barrier Δ=20.9 cm^{-1} (Table 4). Below 2.5 K, the out-of-phase signal revealed two clear peaks associated to at least two relaxation processes which could be explained by the small energy barrier.

One year later, Bernot *et al.* published a second example of Ce^{III}-based SMM of formula $[Ce(DMSO)_8][Ce(NO_3)_2(DMSO)_4(\mathbf{Mo_8O_{26}})_{0.5}][Mo_6O_{19}]$ (**19**) [68]. **19** is obtained by mixing $[(C_4H_9)_4][Mo_6O_{19}]$ with an excess of hydrated $Ce(NO_3)_3$ salt at 60 °C without acidic condition in DMSO (dimethysulfoxide) [70]. Under these conditions, the hexaoxomolybdate can be converted into the octaoxomolybdate polyoxoanion [71]. Thus the final compound revealed the presence of the cationic complex $[Ce(DMSO)_8]^{3+}$, one Lindqvist-type hexaoxomolybdate polyoxoanion and one dinuclear Ce^{III} based complex $[Ce(NO_3)_2(DMSO)_4(Mo_8O_{26})_{0.5}]^-$ (Figure 14). As for **17**, no out-of-phase signal of the magnetic susceptibility is observed without magnetic field while a weak field leads to its appearance (200 Oe). The critical point is the presence of two crystallographically different Ce^{III} ions in D_{3h} and C_{2v} symmetries. The possibility to observe slow magnetic relaxation for the Ce^{III} ion in eight-coordination was discarded due to the low symmetry of the coordination sphere and the isotropic nature of the ligands composing the coordination sphere.

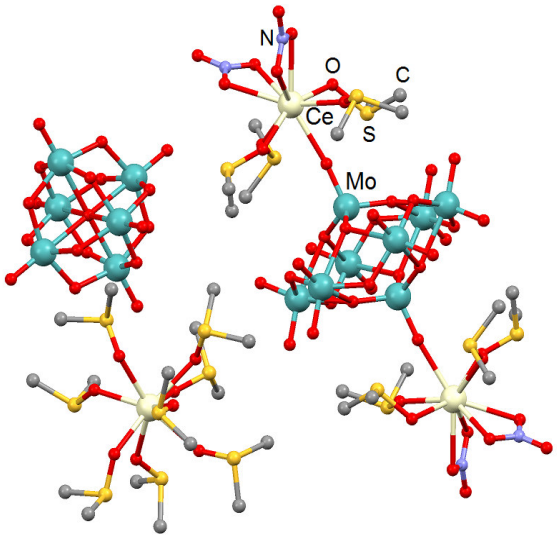

Figure 14. Molecular structure of **19**. Hydrogen atoms are omitted for clarity. Adapted from ref [68].

Once again, in the "high temperature" region a single relaxation time is observed with a SMM behaviour characterised by $\tau_0=2.6\times10^{-7}$ s and $\Delta=24.4$ cm^{-1} (Table 3) while at low temperature another relaxation pathway was observed with $\tau_0=2.1\times10^{-5}$ s and $\Delta=4.4$ cm^{-1} (Table 4). A scan field for compound **19** revealed a third relaxation pathway at higher magnetic field (1400 Oe) with $\tau_0=1.1\times10^{-6}$ s and $\Delta=9.1$ cm^{-1} (Table 4). A Raman process was identified for the magnetic relaxation of **19** at 200 Oe and high temperature region while the participation of a direct process is negligible.

3.2. Neodymium SMMs

The trivalent neodymium ion was not intensively studied for its magnetic properties. In fact, it is a well-known ion for its specific NIR emission making it a good candidate for potential applications in telecommunications or in vivo bio-imaging [72]. Nevertheless, the $Np(COT)_2$ (COT^{2-}=cyclooctatetraene dianion) contains the Np^{IV} ion which has three unpaired *5f*-electrons. This complex behaves as a mononuclear SMM [73] showing that such an ion possesses significant magnetic anisotropy. Thus, the Nd^{III} ion which possesses a $4f^3$ electronic configuration could be also a potential candidate for the elaboration of SMM.

Consequently, Murugesu *et al.* reported the Nd^{III} analogue of **17** formulated as $Li(DME)_3[Nd(\mathbf{L}^{15})_2]$ (**18**) (Figure 13b) [74]. They demonstrated that as expected **18** behaves

as a field-induced SMM with τ_0=5.5×10^{-5} s and Δ=14.6 cm^{-1} (Table 4) due to an adequate ligand field.

18 was however not the first example of Nd^{III}-based SMM since the complex **20** of formula Nd(**L**^{16})$_3$ (**L**^{16}=trispyrazolylborate) (Figure 15) was reported a couple of years before by Rinehart *et al.* [76]. **20** was obtained by reacting $NdCl_3$ salt with K**L**^{16} in water [75,76]. The Nd^{III} ion is surrounded by nine nitrogen atoms and adopts a perfect D_{3h} tricapped trigonal prism as coordination environment.

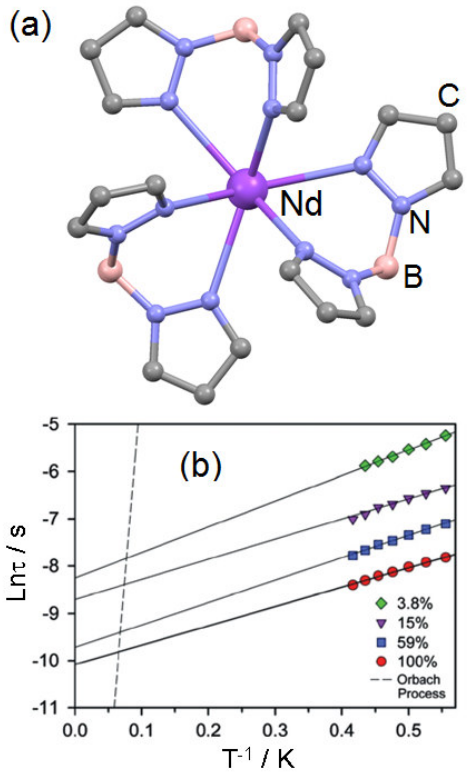

Figure 15. (a) Molecular structure of **20**. Hydrogen atoms are omitted for clarity. (b) Arrhenius plots for different doping values of **20** in a diamagnetic matrix of the La^{III} analogue. Dashed line is given for a pure Orbach process. Green lozenges, purple triangles, blue squares and red full circles are given for a doping of 3.8%, 15%, 59% and pure Neodymium compound. Adapted from ref [76].

20 displayed slow magnetic relaxation under an applied magnetic field of 100 Oe. Nevertheless the energy barrier determined from the variable frequency ac magnetic susceptibility measurements (Δ=2.8 cm^{-1}, Table 4) is much lower than the value determined from the electronic structure obtained through luminescence measurements (119 cm^{-1}) [77]. Since this difference can be due to intermolecular dipolar interactions, nuclear coupling and

mixing of low-lying excited states [34,78-87] a diamagnetic matrix La($\mathbf{L^{16}}$)$_3$ was doped with various percentage of **20**. The most diluted solid-solution led to an energy barrier of 3.8 cm^{-1} that remains far from the expected value extracted from the electronic structure demonstrating that the magnetic relaxation does not involve an Orbach process (Figure 15b). Few months after the publication of Rinehart's article, E. Coronado *et al.* modelled the SMM **20** [88] by a Radial Effective Charge approach (REC) [89]. The radial contraction D_r and charge Z_i have been determined by fitting the experimental spectroscopic data and then used to evaluate the crystal field parameters A_k^q and B_k^q used in the following Hamiltonian: $\hat{H}_{CF} = \sum_{k=2,4,6}\sum_{q=-k}^{k} B_k^q \hat{O}_k^q = \sum_{k=2,4,6}\sum_{q=-k}^{k} \alpha_k (1-\sigma_k) A_k^q \langle r^k \rangle \hat{O}_q^k$ where k is the order of the Stevens operator equivalents $\hat{O}_q^k$, and q is the operator range that varies between k and -k, α_k are the α, β and γ Stevens coefficients for k= 2, 4, 6, respectively, σ_k are the Sternheimer shielding [90] parameters of the *4f* electronic shell and $\langle r^k \rangle$ are the expectation values of r^k. In the previous equation, $A_k^q = \frac{4\pi}{2k+1} C_{kq} (-1)^q \sum_{i=1}^{N} \frac{Z_i e^2 Y_{k-q}(\theta_i, \varphi_i)}{R_i^{k+1}}$ where R_i, θ_i and φ_i are the effective polar coordinates of the point charge, and Z_i is the effective point charge, associated to the *i*-th ligand with the lanthanoid at the origin; e is the electron charge and C_{kq} is a tabulated numerical factor that relates spherical harmonics Y_{k-q} and Stevens operator equivalents. In the specific environment of **20**, the Hamiltonian can be simplified as $\hat{H}_{CF} = \sum_{k=2,4,6} a_k (1-\sigma_k) A_k^0 \langle r^k \rangle \hat{O}_k^0 + \gamma (1-\sigma_6) A_6^6 \langle r^6 \rangle \hat{O}_6^6$. The thermal variation of the magnetic susceptibility of **20** is perfectly reproduced when the ground-state is a mixture of M_J=±5/2 and M_J=±7/2 while the first excited-state is located at 115 cm^{-1} which is in perfect agreement with the energy separation found from the electronic structure.

The first one-dimensional Nd^{III} compound which displayed slow magnetic relaxation was proposed by Arauzo *et al.* in 2014 [91]. {[Nd_2($\mathbf{L^{17}}$)$_6$(H_2O)$_4$]·2H_2O}$_n$ (**21**, Figure 16a) was obtained by mixing cyanoacetic acid (H$\mathbf{L^{17}}$, Scheme 3) and neodymium oxide in aqueous media [92].

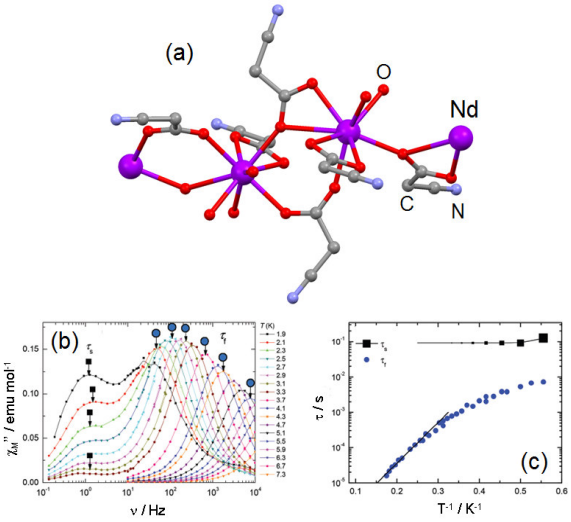

Figure 16. (a) Molecular structure of $\{[Nd_2(\mathbf{L}^{17})_6(H_2O)_4]\}_n$. Hydrogen atoms and water molecules of crystallisation are omitted for clarity. (b) Frequency dependence of the imaginary component of the magnetic susceptibility at H=1500 Oe. (c) Thermal dependence of the relaxation time for both processes found for **21** at H=1500 Oe determined from Figure 16b. Full black squares and full blue circles represented the τ_S (slow relaxations) and τ_f (fast relaxations) respectively. Adapted from ref [91].

On the basis of *ab-initio* calculations, the relative energies of the five Kramers doublets have been determined giving an energy separation of 72.3 cm^{-1} between the ground- and first excited-states (Table 4) as well as *g* factor contributions of g_x=0.3, g_y=1.2 and g_z=3.9. These characteristics highlighted an important magnetic anisotropy for the Nd^{III} ion in **21**. The experimental ac susceptibility measurements did not show any slow magnetic relaxation without applied magnetic field due to i) the transversal component of the magnetic anisotropy or/and ii) dipolar interactions with the neighbouring Nd^{III} ions of the chain. Nevertheless, applying an optimal field of 1500 Oe led to the observation of the expected slow magnetic relaxation (Figure 16b). Two relaxation processes were identified. The slowest one was attributed to a direct relaxation process (full black squares in Figure 16c) while below 3K the relaxation mechanism was attributed to Orbach relaxation. However, the clear discrepancy between the experimental energy barrier (18.5 cm^{-1}) and the calculated one (72.3 cm^{-1}) could be thought of as a coexistence of several processes and not an exclusive Orbach process. In any case, it is clear that both direct and Orbach processes are operating under an applied field as already detected by means of EPR measurements in the 1960s [93]. Finally, even if in a structural point of view, **21** is described as a chain, in a magnetic point of view, **21** should be

viewed as a 1D assembly of mononuclear Nd^{III} SMMs. It is worth to noticing that the Gd^{III} analogue displayed also slow magnetic relaxation while the Gd^{III} ion is an isotropic ion in a magnetic point of view [91].

One year later, two other Nd^{III}-based 1D compounds which displayed slow magnetic relaxation were published [94]. Both structures have been obtained from the 3,5- (**L**^{18}, Scheme 3) and 2,4-dinitrobenzoic acids (**L**^{19}, Scheme 3).

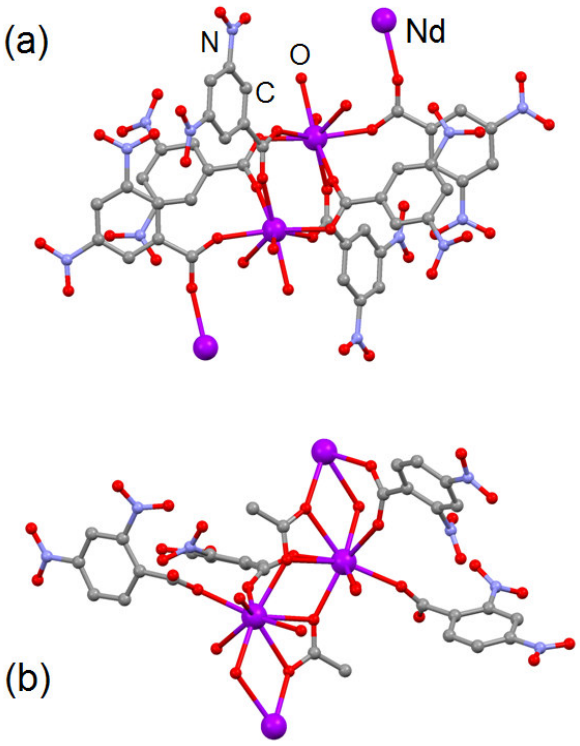

Figure 17. Molecular structures of $\{[Nd(\mathbf{L}^{18})_3(H_2O)_2]\}_n$ (a) and **23** (b). Hydrogen atoms and solvent molecules of crystallisation have been omitted for clarity. Adapted from ref [94].

$\{[Nd(\mathbf{L}^{18})_3(H_2O)_2]\cdot 2CH_3CN\}_n$ (**22**) and $\{[Nd(\mathbf{L}^{19})_2(CH_3COO)(H_2O)_2]\}_n$ (**23**) (Figure 17) behave similarly to the previous reviewed chain (**21**) since slow magnetic relaxation is observed only under magnetic field because significant transversal components are still present (g_x=1.02, g_y=2.01 and g_z=3.5 and g_x=0.62, g_y=1.73 and g_z=4.12 for **22** and **23**, respectively). The activation energy barriers are close (19 cm^{-1} and 20 cm^{-1} for **22** and **23** versus 18.5 cm^{-1} for **21**) and once again the calculated values (77.8 cm^{-1} and 87.3 cm^{-1} for **22** and **23**) are much higher than the experimental ones but in the same order of magnitude than the calculated value for **21** (72.3 cm^{-1}) (Table 4).

3.3. Holmium SMMs

The lanthanide mononuclear SMM started in 2003 with the association of a Dy^{III} ion and double Decker ligands [95], while the first uncommon lanthanide ion involved in a SMM was Ho^{III} in 2005 [96]. Even if it was used before Yb^{III} or Nd^{III}, the Ho^{III}-based SMMs are still very rare in the literature probably due to its 100% natural abundance I=7/2 which allows rapid quantum tunnelling due to hyperfine interaction in coordination complexes [96] and in inorganic lattices [97]. One can take in his mind that the rarity of Ho^{III}-based SMM can be due to the non-Kramers nature of such lanthanide, which places constraints on the symmetry of the coordination environment needed for SMM behaviour, and to the fact the 4f electron density is not very anisotropic.

TBA[Ho($\mathbf{L^{20}}$)$_2$] (**24**) (where TBA is tetrabutylamonium) compound was prepared from conventional synthetic methods [98-99] (Figure 18, Scheme 3).

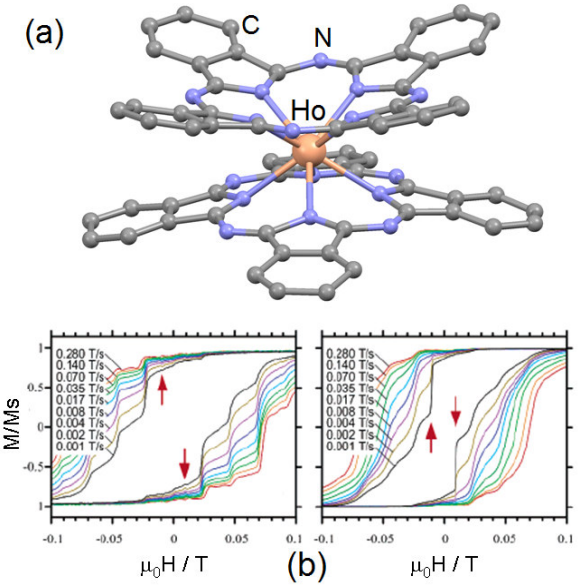

Figure 18. (a) Molecular structure of [Ho($\mathbf{L^{20}}$)$_2$]$^-$. Hydrogen and TBA$^+$ cation are omitted for clarity. (b) Field-dependence of the magnetization at different temperature and field scan rate for 2% of **24** in a diamagnetic matrix of TBA[Y($\mathbf{L^{20}}$)$_2$]. Adapted from ref [96].

24 behaves as a SMM with an energy separation between the ground- ($M_J = \pm 5$) and first excited-states of 15 cm^{-1} [97]. Then the mononuclear TBA[Y($\mathbf{L^{20}}$)$_2$] complex was doped with 2% of **24** based on the very similar ionic radius of Ho^{III} and Y^{III} ions [99]. The field-dependence of the magnetization for the resulting compound was studied by micro-SQUID technique and an open hysteresis was observed below 0.5 K while a staircase-like structure

was observed for the hysteresis loop at 0.04 K [96]. This structure was proving the QTM in **24**. The quantum process was attributed to resonant quantum tunnelling between entangled states of the electronic and nuclear spin systems.

In 2009, Coronado *et al.* studied two series of lanthanide-based POM [24]. Complex **1** was already reviewed as an Yb^{III}-based SMM (see Section 2). The Ho^{III} analogue ($Na_{13}[Ho(\mathbf{SiW_{11}O_{39}})_2]$ (**25**)) behaves as a mononuclear SMM with an energy barrier of 6 cm^{-1} between the ground- (M_J=±4) and first excited-states (M_J=±5) [24]. More interesting is the second Ho^{III}-based POM ($Na_9[Ho(\mathbf{W_5O_{18}})_2]$ (**26**, Figure 19a).

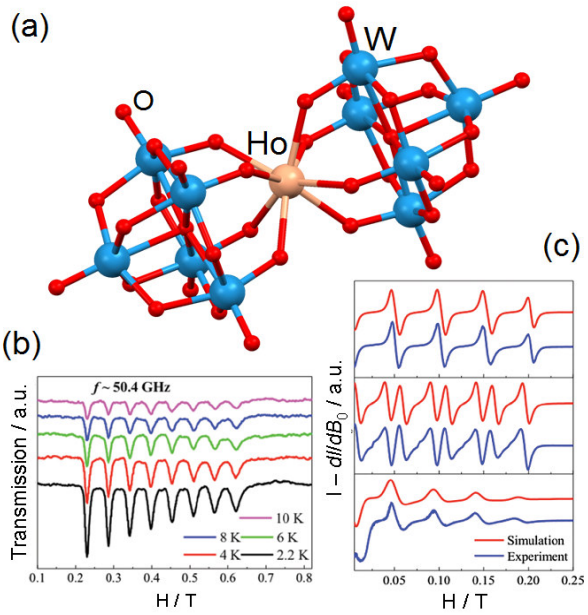

Figure 19. (a) Molecular structure of $[Ho(\mathbf{W_5O_{18}})_2]^{9-}$. Sodium cations and water molecule of crystallisation are omitted for clarity. (b) Temperature dependent high-frequency EPR spectrum for the $Na_9[Ho_{0.25}Y_{0.75}(\mathbf{W_5O_{18}})_2]$ sample between 2.2 and 10 K. (c) From up to down: Experimental (blue line) and simulated (red line) X-band EPR spectra using the 9.64 GHz perpendicular excitation mode for $Na_9[Ho_{0.1}Y_{0.9}(\mathbf{W_5O_{18}})_2]$, parallel excitation mode for $Na_9[Ho_{0.1}Y_{0.9}(\mathbf{W_5O_{18}})_2]$, and perpendicular excitation mode for **26**. Adapted from ref [101].

26 behaves as a SMM with a quite higher energy barrier of 16 cm^{-1} than in **25**. Since the crystal field around the Ho^{III} ion is similar in both compounds, the nature of the ground-state is unsurprisingly found identical (M_J=±4). **26** was studied by multi-frequency EPR few years later [101]. The EPR study confirmed the M_J=±4 ground-state which is split into eight M_I sub-levels through the hyperfine coupling to I=7/2 nuclear spin. The M_J=±4 ground state is

efficiently connected via the large tunnelling gap of 9 GHz at zero magnetic field. This large tunnelling gap allows the possibility of observing coherent zero-field tunnelling dynamics. This work opened the route to the study of such systems by pulsed EPR measurements in order to evaluate their suitability as spin qubits.

A Ho^{III}-based Preyssler anion was reported by the same group almost concomitantly [102]. This mononuclear compound was formulated as $K_{12}[Ho(H_2O)\mathbf{P_5W_{30}O_{110}}]\cdot nH_2O$ (**27**) (Figure 20a) where the Ho^{III} ions occupied two different sites of coordination in a 5-fold geometry formed by five phosphate oxygens, five bridging oxygens between two tungsten atoms and one axial water molecule. It resulted an eleven coordination number and a monocapped pentagonal antiprism as coordination sphere symmetry for the Ho^{III} ion. The Crystal Field parameters were determined using the dc magnetic measurements. Due to the C_5 symmetry, the CF Hamiltonian could be simplified as the following: $\hat{H} = \alpha A_2^0 r^2 \hat{O}_2^0 + \beta A_4^0 r^4 \hat{O}_4^0 + \gamma A_6^0 r^6 \hat{O}_6^0 + \gamma A_6^5 r^6 \hat{O}_6^5$. The best reproduction of the thermal variation of the magnetic susceptibility of **27** gave the doublet M_J=±8 as the ground-state while the first doublet excited-state is localised 14 cm^{-1} above and has been identified as a mixture of M_J=±5 and M_J=±0. The nature of the doublet ground-state for **27** allowed the possibility to observe an SMM behaviour at low temperature. Such behaviour was highlighted by ac magnetic measurements and the activation energy is 0.6 cm^{-1} which is much lower than the value found on the basis of the electronic structure determined from the fit of dc measurements (Table 4). This very small value was explained by the high efficiency of the quantum tunnelling which is promoted by the strong hyperfine coupling due to the 100% I=7/2 for an Ho^{III} ion. In other words, the quantum tunnelling transitions between the M_J states with opposite sign are induced by level crossings between states of equal M_I under an applied magnetic field. Finally the very long relaxation time (τ_0=6×10^{-3} s) was associated with the lifetime of excited nuclear spin states and it was compatible with the weak interaction between the nuclear spin and the lattice.

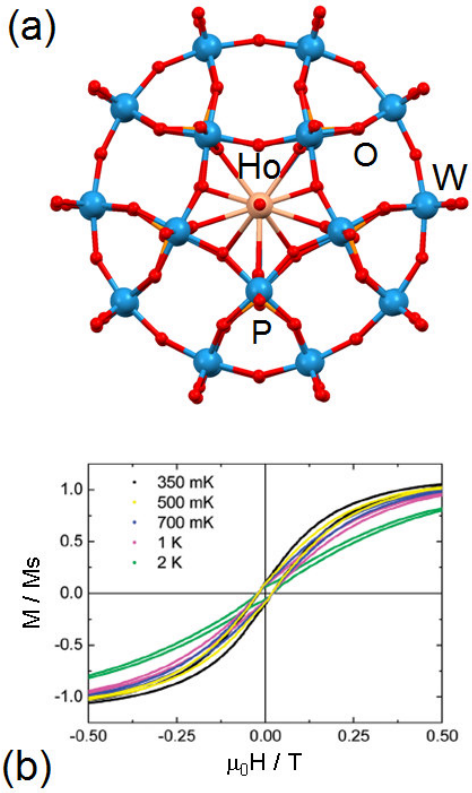

Figure 20. (a) Molecular structure of $[Ho(H_2O)\mathbf{P_5W_{30}O_{110}}]^{12-}$. Hydrogen atoms, cations and water molecules of crystallisation have been omitted for clarity. (b) Magnetization hysteresis loops of **27** measured between 0.35 and 2 K. The sweeping rate of the magnetic field was 0.54 T min^{-1}. Adapted from ref [102].

Interestingly, magnetic bistability was observed at low temperature (below 2 K) for **27** (Figure 20b). The difference between the blocking temperature and the energy at which the magnetic bistability is observed was explained by the increase of the magnetic relaxation with the magnetic field [82,84].

Until now, to the best of our knowledge, only one pure Ho^{III} polynuclear SMM has been reported by McInnes *et al.* [103]. The pentanuclear complex of formula $[Ho_5O(OiPr)_{13}]$ (**28**) was obtained by reaction between freshly synthesized KO^iPr and anhydrous $HoCl_3$ with addition of stoichiometric amount of H_2O (Figure 21a). **28** displayed temperature dependence of its magnetic susceptibility below 40 K but without clear maxima in a zero-applied magnetic field. Applying an optimal field (5.5 kOe), clear maxima are observed below 33 K allowing the determination of the dynamic parameters Δ=278 cm^{-1} and $\tau_0=1.5\times10^{-9}$ s (Figure 21b). It is worth to notice that this energy barrier was among the highest yet observed for a lanthanide SMM in 2011. The change of dynamic magnetic behaviour of **28** in applied field

was explained by the expected strength of the Ho^{III} hyperfine coupling (*ca.* 0.04 cm^{-1}) which is quenched in an applied field above *ca.* 0.2 T.

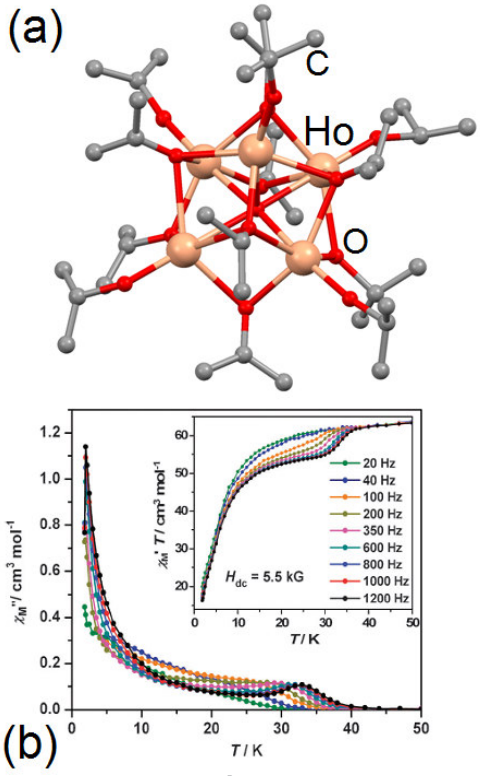

Figure 21. (a) Molecular structure of **28**. Hydrogen atoms are omitted for clarity. (b) Temperature dependence of the out-of-phase component of the magnetic susceptibility in an applied field of 5.5 kOe. In inset, Temperature dependence of the in-phase component of the magnetic susceptibility in an applied field of 5.5 kOe. The applied frequencies ranged from 20 to 1200 Hz. Adapted from ref [103].

3.4. Thulium SMM

Non-Kramers ions are very scarce in the elaboration of SMMs except for Tb^{III} [104-108]. We already reviewed few Ho^{III} SMMs (see previous section) and some examples with Tm^{III} also exist. Gao *et al.* associated an equatorial ligand such as COT ligand (**L**^{21}, Scheme 3) in order to satisfy the Ising limit condition for a lanthanide ion with a prolate electron density. Such an approach was already successful in the case of the Kramers Er^{III} ion [109-112]. Nevertheless the challenge is more difficult in the case of a non Kramers prolate ion such as Tm^{III} ion because no thulium complexes could show slow magnetic relaxation under zero dc field even the thulium complexes featuring high molecular symmetry [113]-[115]. As said for the Ho^{III} ion, this fact could be due to the non-Kramers nature of such ion and the

difficulties to satisfy the coordination environment symmetry constraints for the prolate shape of electron density of $M_J = \pm 6$. The two resulting complexes [(Tp)Tm($\mathbf{L^{21}}$)] (**29**) (where Tp=hydrotris(1-pyrazolyl)borate) and [(Tp*)Tm($\mathbf{L^{21}}$)] (**30**) (where Tp*=hydrotris(3,5-dimethyl-1-pyrazolyl)borate) (Figure 22a) are the first Tm^{III} mononuclear complexes which displayed SMM behaviour [116]. They have been obtained by modifying the historical synthetic method [117] by starting from the halide precursor [$\mathbf{L^{21}}$]Tm(Cl)(THF)]$_2$ which reacts with KTp or KTp* in THF.

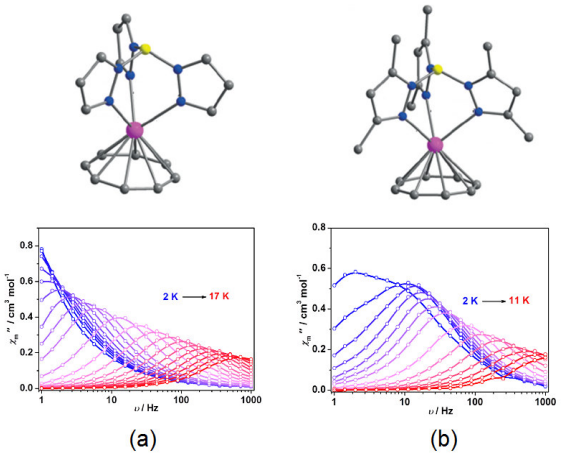

Figure 22. (a) Molecular structure of **29** and Frequency dependence of the magnetic susceptibility of **29** under an applied field of 2000 Oe between 2 and 17 K. (b) Molecular structure of **30** and Frequency dependence of the magnetic susceptibility of **30** under an applied field of 2000 Oe between 2 and 11 K. Adapted from ref [116].

In a zero-magnetic field, the QTM is too efficient to permit the observation of an out-of-phase signal of the magnetic susceptibility while applying 2 kOe, SMM behaviour appeared for both compounds (Figure 22). The magnetic data for **29** could be fitted by a combination of one Raman process and one Orbach process giving an energy barrier of 90.4 cm^{-1} and a pre-exponential factor of $\tau_0=4.7\times10^{-7}$ s (Table 4). The situation for **30** is different since the application of a similar model did not permit to fit the magnetic data. In fact the adequate combination was found with both Raman and QTM processes. Then *ab-initio* calculations were performed to explain why **29** is a better SMM than **30**. A faster QTM was found for **30** than **29** and a more important mixing of M_J states in the composition of the doublet ground-state for **30** than **29** due to the steric hindrance of Tp* compare to Tp which breaks the C_3 symmetry. Finally frequency dependence of the magnetic susceptibility could

be observed without applied magnetic field when doping an isomorphous diamagnetic matrix with **29**. This result proves that dipole-dipole interactions are source of QTM in **t**his compound.

The beginning of this review demonstrated that uncommon lanthanide in the design of SMM such as Ce^{III}, Nd^{III}, Ho^{III} and Tm^{III} are moving slowly out of their niche. All of the described complexes highlighted significant magnetic anisotropy even if pure Ising system is not yet reached since the remaining transversal components induce QTM. In the case of the oblate Ce^{III} and Nd^{III} ions a very small magnetic field is enough to cancel the QTM and to observe interesting SMM behaviour. The involved mechanisms in the relaxation of the magnetization in these complexes are a mix between Orbach, Direct and Raman processes without clear trends. The nature of the processes is strongly complex-dependent and especially depends on the nature of the lanthanide ion. In the case of the Ho^{III}-based SMM, the QTM is allowed by mixing the M_I states due to the intense hyperfine coupling coming from the 100 % I=7/2 of the Ho^{III} ion. For the Tm^{III}-based SMM, the QTM comes from the dipole-dipole interactions. Finally, it has been demonstrated that Ho^{III} SMMs could be good candidates for molecular spintronics applications, another ever-growing field of research [118-123].

4. Heterobinuclear Zinc-Lanthanide SMMs: Borderline cases of purely 4f SMMs

4.1. ZnYb SMMs

The Zn^{II} ion possesses a $3d^{10}$ electronic configuration and can be considered as silent in a magnetic point of view. Nevertheless in an electronic point of view the association of such an ion with a lanthanide ion results in a 3*d*4*f* heterobimetallic sample. Therefore such compounds are qualified as borderline cases in this review. Two main reasons justify the association of a diamagnetic ion, such as Zn^{II}, with a lanthanide ion to build SMMs: i) the Zn^{II} metallo-precursors are used as structural agents or building blocks to control the coordination site of the lanthanide and consequently its symmetry, ii) the Zn^{II} building blocks are used as metallo-chromophores for the sensitization of the lanthanide ion.

Table 5. Heterobinuclear Zinc-Lanthanide SMMs (Ln=Ce^{III} and Yb^{III})

ZnLn-SMM	Δ/cm^{-1}	τ_0/s	H/Oe	M_J ground	ref

				state[e]	
(**31**)*	9[a]/112[b]/109[c]	9.3×10^{-7}	600	±5/2	[124]
(**32**)*	16[a]/169[b]/116[c]	3.9×10^{-7}	600	±5/2	[124]
$[Zn_3Yb(\mathbf{L^{23}})(NO_3)_3]\cdot4CH_3OH$ (**33**)	12[a]	4.8×10^{-6}	500	-	[129]
(**34**)*	13.5[a]/315[b]/1[c]	3.1×10^{-6}	1000	±7/2	[131]
$[Zn(\mathbf{L^{24}})(NO_3)Yb(NO_3)_2]$ (**35**)	18.8[a]/303[b]/0.1[c]	8.8×10^{-7}	1000	±7/2	[131]
$[Ce(ZnI(\mathbf{L^{25}}))_2](BPh_4)\cdot CH_3OH$ (**36**)	14.7[a]/240[c]/180[d]	1.6×10^{-7}	0-100	±5/2	[132]

[a] Effective energy barrier determined from ac measurements. [b] Effective energy barrier determined from luminescence measurements. [c] Effective energy barrier determined from dc measurements. [d] Effective energy barrier predicted by *ab initio* calculations. [e] When the ground state M_J value is not given is because it was not determined in the corresponding article. * (**31**) $=[YbZn_4(\mathbf{L^{22}})_4(py)_4(DMF)_4](CF_3SO_3)_3\cdot5DMF\cdot7H_2O$, (**32**) $=[YbZn_4(\mathbf{L^{22}})_4(iqn)_4(DMF)_4](CF_3SO_3)_3\cdot6DMF\cdot4H_2O$, (**34**) $=[Zn(\mathbf{L^{24}})Yb(H_2O)(CO_3)]_2(NO_3)_2\cdot4CH_3OH$

The first example of ZnLn heterobimetallic compound presented herein is typical of this series of molecules. Tong *et al.* used the [12-metallacrown-4] discovered by Pecoraro and Lah [125-128] to create appropriate LF environment by taking advantage of its 4-fold axis [124]. The central cavity of [12-metallacrown-4] is then suitable for coordination of lanthanide ions.

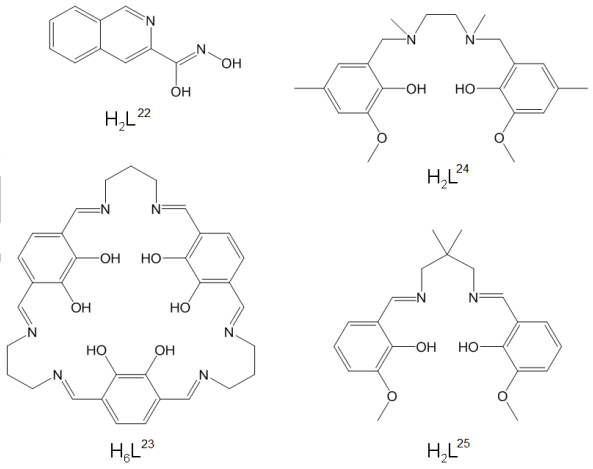

Scheme 4. Structures of selected ligands used to elaborate the $Zn^{II}Yb^{III}$ and $Zn^{II}Ce^{III}$ heterobimetallic SMMs.

The reaction between quinaldichydroxamic acid ($\mathbf{L^{22}}$) (Scheme 4), Zn^{II} triflate, Yb^{III} triflate, triethylamine in DMF leads to the formation of $[YbZn_4(\mathbf{L^{22}})_4(py)_4(DMF)_4](CF_3SO_3)_3\cdot5DMF\cdot7H_2O$ (**31**) and

$[YbZn_4(\mathbf{L}^{22})_4(iqn)_4(DMF)_4](CF_3SO_3)_3{\cdot}6DMF{\cdot}4H_2O$ (**32**) when pyridine (py) or isoquinoline (iqn) was added during the crystallization, respectively (Figure 23).

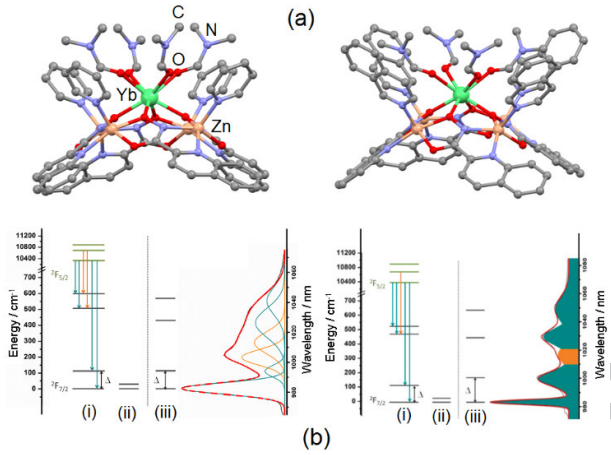

Figure 23. (a) Molecular structures of $[YbZn_4(\mathbf{L}^{22})_4(py)_4(DMF)_4]^{3+}$ (left) and $[YbZn_4(\mathbf{L}^{22})_4(iqn)_4(DMF)_4]^{3+}$ (right). Hydrogen atoms, triflate anions and solvent molecules of crystallisation have been omitted for clarity. (b) Correlations of the different set of data for the energy levels of the $^2F_{7/2}$ ground state multiplet obtained from dc fit (i) ac fit (ii) and luminescence spectra (iii) for **31** (left and **32** (right). Adapted from ref [124].

The two compounds have similar crystallographic structures with the formation of the [12-MC-4] metallacrown which is formed by four ditopic ligands ($\mathbf{L}^{22}$) bridging the four Zn^{II} ions. The Yb^{III} ion is sandwiched between four oxygen atoms coming from the metallacrown and four oxygen atoms coming from four coordinated DMF molecules. The distinction between both structures is the nature of the axial ligand coordinated to the Zn^{II} ion, *i.e.* pyridine for **31**, isoquinoline for **32**. The coordination sphere around the Yb^{III} ion can be described as a slightly distorted square antiprism. Then the physical properties of the two compounds were studied using the same approach than for compounds **3**, **6** and **10**. The originality of the work comes from the light irradiation of the metallacrown to sensitize the Yb^{III} luminescence. The dc data were fitted using a Stevens approach considering the following Hamiltonian: $\hat{H} = B_2^0\hat{O}_2^0 + B_4^0\hat{O}_4^0 + B_4^4\hat{O}_4^4 + B_6^0\hat{O}_6^0 + B_6^4\hat{O}_6^4$. For both compounds the ground-states are identified as M_J=±5/2 and the activation energy (116 cm^{-1} and 109 cm^{-1} for **31** and **32,** respectively) are in agreement with the energy separation of the luminescence spectra (112 cm^{-1} and 169 cm^{-1} for **31** and **32,** respectively) (Figure 23b). As for the pure Yb^{III} SMMs, the thermally activated relaxation process (Orbach) was excluded because the

extracted energy barrier from the ac data gave values much smaller (9 cm^{-1} and 16 cm^{-1} for **31** and **32,** respectively) than the ones extracted from luminescence spectra and dc data (Table 5).

It is worth to notice that **31** and **32** were not the first $Zn^{II}Yb^{III}$ heterobimetallic compounds that exhibit SMM behaviour. Indeed, the first one was reported in 2011 by Powell *et al.* [129]. The $[Zn_3Yb(\mathbf{L}^{23})(NO_3)_3]\cdot 4CH_3OH$ (**33**) compound (Figure 24a) was synthesized starting from the dialdehyde 1,4-diformyl-2,3-dihydrobenzene, acetate of Zn^{II} and 1,3-diaminopropane in a mixture of alcohols (MeOH/isopropanol). The SMM behaviour was observed after quenching of the QTM by an applied magnetic field of 500 Oe (Figure 24b) and the extracted dynamic parameters are very similar to those observed for compounds **31** and **32** (Δ=12 cm^{-1} and $\tau_0=4.8\times10^{-6}$ s). Two relaxation pathways were identified and the set of data was obtained using Christou's non-linear Arrhenius plots [130]. Unfortunately no correlation was done between the luminescence spectrum and CF parameters for **33**.

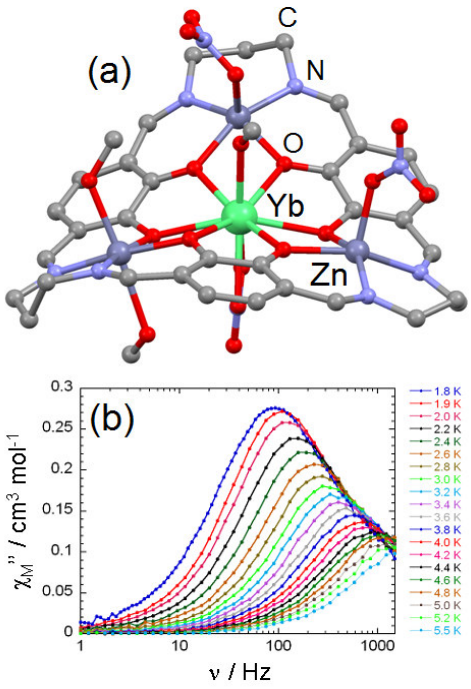

Figure 24. (a) Molecular structure of $[Zn_3Yb(\mathbf{L}^{23})(NO_3)_3]$. Hydrogen atoms and methanol molecules of crystallisation have been omitted for clarity. (b) Frequency dependence of the magnetic susceptibility between 1.8 and 5.5 K. Adapted from ref [129].

Recently, two new $Zn^{II}Yb^{III}$ heterobimetallic compounds were reported by Colacio *et al.* [131]. $[Zn(\mathbf{L}^{24})Yb(H_2O)(CO_3)]_2(NO_3)_2\cdot 4CH_3OH$ (**34**) and $[Zn(\mathbf{L}^{24})(NO_3)Yb(NO_3)_2]$ (**35**) complexes have been obtained from the Schiff base $\mathbf{L}^{24}$ and their crystallographic structures

are depicted in Figure 25a. The following CF Hamiltonian $\hat{H}_{CF} = \sum_{i=1}^{2} B_2^0\hat{O}_2^0 + B_4^0\hat{O}_4^0 + B_4^4\hat{O}_4^4 + B_6^0\hat{O}_6^0 + B_6^4\hat{O}_6^4 - 2J\ \hat{J}_1\cdot\hat{J}_2 + \beta g_J\left(\hat{J}_1+\hat{J}_2\right)\cdot\vec{H}$, the sensitization of the Yb^{III} luminescence and the dynamic magnetic properties permitted to extract three sets of data for the energy splitting of the $^2F_{7/2}$ multiplet ground-state (see Table 5). Interestingly, both compounds have the highest M_J value (M_J=±7/2) as ground-state with the first excited-state very close in energy (<1 cm^{-1}). It is worth noticing that they are only the second and third examples after compound **10** which are able to stabilize such M_J states values. As observed for the previous examples of Yb^{III} SMMs, the activation energies extracted from the luminescence spectra are much higher than those extracted from the magnetic data due to the nature of the magnetic relaxation processes. For these present cases, the magnetic relaxation takes place through a combination of QTM and Raman processes (Figure 25b).

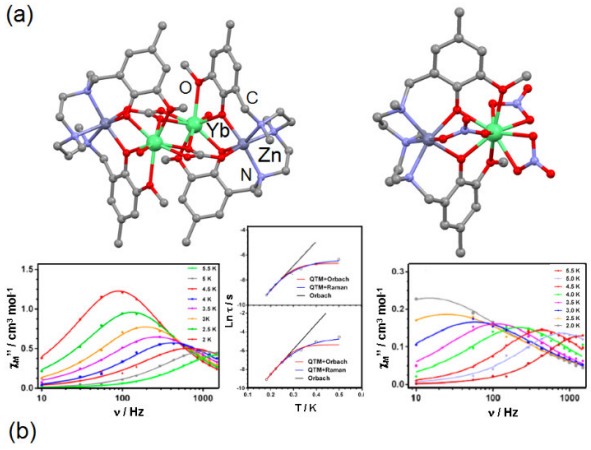

Figure 25. (a) Molecular structures of $([Zn(\mathbf{L}^{24})Yb(H_2O)(CO_3)]_2)2^+$ and **35**. Hydrogen atoms, anions and solvent molecules of crystallisation have been omitted for clarity. (b) Frequency dependences of the magnetic susceptibilities in the 2-5.5 K temperature range and Arrhenius plots (red line, blue line and black line are representative of QTM+Orbach, QTM+Raman and Orbach respectively). Adapted from ref [131].

4.2. ZnCe SMM

Similar strategy than for Yb^{III} ion was used for Ce^{III} ion. Thus the $[Ce(ZnI(\mathbf{L}^{25}))_2](BPh_4)\cdot CH_3OH$ (**36**) compound was studied by Kajiwara *et al.* [132]. The X-ray structure of this trinuclear complex highlighted a Ce^{III} ion in a O_9 environment (Figure 26a). The dynamical magnetic properties showed a SMM behaviour without applied magnetic field (Figure 26b(i)). Such behaviour was not observed for the two previous Ce^{III}-

based SMMs **17** and **19**. Two years later, G. Rajaraman theoretically studied the magnetic properties of complex **36** and explained that the presence of diamagnetic Zn^{II} ions increases the charge on the phenoxo oxygen atoms enhancing the activation barrier and the slow magnetic relaxation [133]. Obviously, the QTM was partially quenched using a weak magnetic field of 50 and 100 Oe (Figures 26b (ii) and (iii)). The magnetic susceptibility was reproduced using the simple Hamiltonian $\hat{H} = B_2^0\hat{O}_2^0 + B_4^0\hat{O}_4^0$ giving the M_J=±5/2 as the doublet ground-state and an energy barrier of 240 cm^{-1}. As already observed, the discrepancy between the activation energy found with the ac and dc magnetic measurements suggested that the relaxation mechanism would not be only a two-phonon Orbach process. *Ab-initio* calculations corroborated the nature of the doublet ground-state (M_J=±5/2) with significant mixing with M_J=±3/2 due to the low-symmetry environment of the Ce^{III} ion in **36**. The calculated energy barrier (180 cm^{-1}) is much higher than the experimental value of 14.7 cm^{-1} determined from the ac data but in agreement with the 240 cm^{-1} determined from the dc data (Table 5).

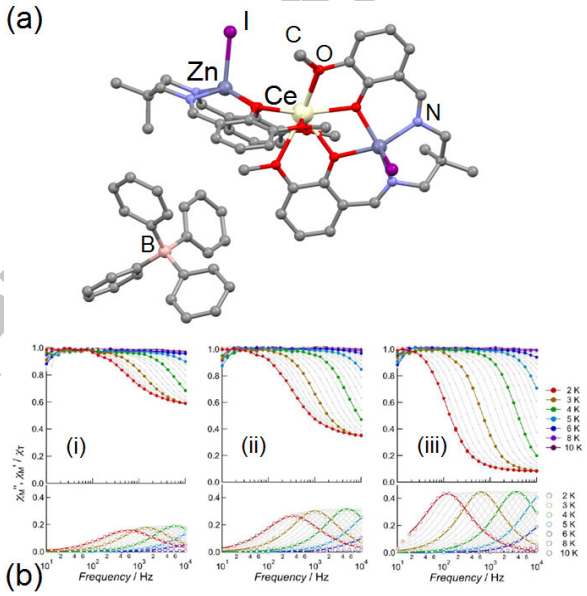

Figure 26. (a) Molecular structure of $[Ce(ZnI(\mathbf{L}^{25}))_2](BPh_4)$. Hydrogen atoms and methanol molecules of crystallisation are omitted for clarity. (b) Frequency dependence of the normalised magnetic susceptibilities measured under (i) 0 Oe, (ii) 50 Oe and (iii) 100 Oe applied magnetic field in a 2-10 K temperature range. Adapted from ref [132].

In conclusion for this section, the association of diamagnetic ions such as the $3d^{10}$ Zn^{II} at least preserves the SMM behaviour and the slow magnetic mechanisms and even seems to be a good way to structurally control the final compounds as well as to enhance the magnetic properties by electrostatic effects.

5. Heterobimetallic 4*f*4*f*' Lanthanide SMMs

In this last section, two heterebimetallic 4f4f' SMMs are presented.

Table 6. Heterobinuclear Lanthanide SMMs (Ln=Dy^{III} and Yb^{III})

DyYb-SMM	Δ/cm^{-1}	τ_0/s	H/Oe	M_J ground state[e]	ref
$[Yb_2(\mathbf{L^{26}})_2Cl_4(H_2O)(MeCN)]\cdot CH_3CN$ (**37**)	14.7[a]/177.4[d]	9.3×10^{-7}	3500	-	[134]
$[Dy_{0.87}Yb_{1.13}(\mathbf{L^{26}})_2Cl_4(H_2O)(MeCN)]\cdot CH_3CN$ (**39**)	20.2[a]	3.9×10^{-7}	3500	-	[134]
$(HNEt_3)[Yb(\mathbf{L^{27}})_2]$ (**40**)	17.5[a]/98.8[b]/56.8[c]	-	1800	-	[135]
$(HNEt_3)[Dy_{0.135}Yb_{0.865}(\mathbf{L^{27}})_2]$ (**42**)	7.1[a]	-	1800	-	[135]

[a] Effective energy barrier determined from ac measurements. [b] Effective energy barrier determined from luminescence measurements. [c] Effective energy barrier determined from dc measurements. [d] Effective energy barrier predicted by *ab initio* calculations. [e] The ground state M_J values were not determined in the corresponding article.

The first system is made from the association of the Yb^{III} ion with the 1,3,5-cyclohexanetriol ligand (H$\mathbf{L^{26}}$, Scheme 5) [134].

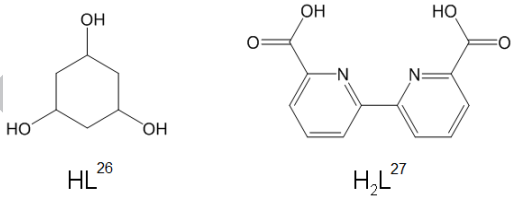

Scheme 5. Structures of selected ligands used to elaborate the heterobimetallic SMMs.

The X-ray structure of the complex $[Yb_2(\mathbf{L^{26}})_2Cl_4(H_2O)(MeCN)]\cdot CH_3CN$ (**37**) features two Yb^{III} ions in a seven-coordination environment due to the four $\mathbf{L^{26}}$ ligands (two protonated and two deprotonated), two chloride anions and a disordered MeCN/H_2O molecules (Figure 27). The coordination sphere lies between capped-octahedron (C_{3v}) and capped trigonal prism (C_{2v}). **37** has been identified as a SMM with Δ=14.7 cm^{-1} and $\tau_0=9.3\times10^{-7}$ s with the slow magnetic relaxation occurring through a direct process. The Dy^{III} analogue (**38**) was also synthesized and it behaves as a SMM with Δ=86.2 cm^{-1}. Finally they substituted one Yb^{III} ion by one Dy^{III} ion leading to the heterobimetallic

$[Dy_{0.87}Yb_{1.13}(\mathbf{L}^{26})_2Cl_4(H_2O)(MeCN)]\cdot CH_3CN$ (**39**) complex. An analysis of the magnetic properties showed an enhancement of the activation energy for the Yb^{III} centre in **39** (from 14.7 cm^{-1} to 20.2 cm^{-1}) while this parameter decreased from 86.2 cm^{-1} to 69.5 cm^{-1} for the Dy^{III} centre. These variations were attributed to small geometrical evolutions in the environment of the lanthanide ions.

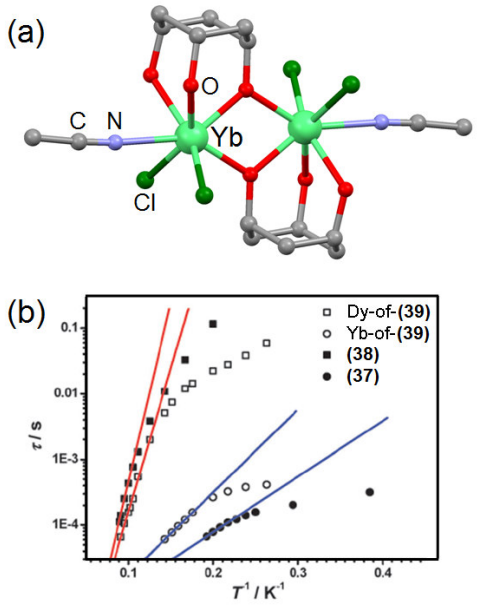

Figure 27. (a) Molecular structure of $[Yb_2(\mathbf{L}^{26})_2Cl_4(H_2O)(MeCN)]$. Hydrogen atoms and MeCN molecule of crystallisation were omitted for clarity. (b) Arrhenius plots in a dc field of 3500 Oe for dinuclear complexes **37**, **38** and **39**. Adapted from ref [134].

The second example of heterobimetallic *4f4f'* complexes was published by M.-L. Tong the same year [135]. The pure Yb^{III} analogue was obtained by the reaction between $Ln(NO_3)_3\cdot 6H_2O$ and 2,2'-bipyridine-6,6'-dicarboxylic acid ($H_2\mathbf{L}^{27}$, Scheme 5) in presence of Et_3N. The resulting $(HNEt_3)[Yb(\mathbf{L}^{27})_2]$ (**40**) complex revealed an Yb^{III} ion in a trigonal dodecahedron geometry (D_{2d} symmetry) (Figure 28a). **40** has been identified as a SMM with Δ=17.5 cm^{-1} with the slow magnetic relaxation occurring through direct and/or Raman process(es). In case of **40**, the dc data provided another value for the energy activation (56.8 cm^{-1}) as well as the photophysical properties (98.8 cm^{-1}) (Table 6) since the ligand $\mathbf{L}^{27}$ is suitable for the Yb^{III} luminescence sensitization. The Dy^{III} analogue (**41**) behaves also as a SMM with Δ=38 cm^{-1} with a magnetic relaxation occurring through Orbach process. In the mixed spin compound $(HNEt_3)[Dy_{0.135}Yb_{0.865}(\mathbf{L}^{27})_2]$ (**42**), the two lanthanide ions highlighted slow magnetic relaxation but with higher (47 cm^{-1}) and lower (7.1 cm^{-1}) energy activations for

Dy^{III} and Yb^{III} ions, respectively. This result is in contradiction with the previous example (**39**). Such behaviour was explained by the reduction (in the case of the Dy^{III} ion) and increase (in the case of the Yb^{III} ion) of the dipole-dipole interactions due to the dilution of the Dy^{III} ion in the paramagnetic Yb^{III} matrix.

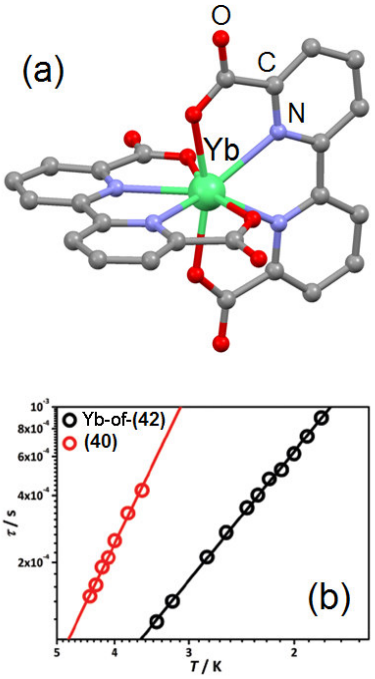

Figure 28. (a) Molecular structure of $[Yb(\mathbf{L}^{27})_2]^-$. Hydrogen atoms and cation are omitted for clarity. (b) Arrhenius plots for complexes **40** and **42** under an applied field of 1800 Oe. Adapted from ref [135].

6. Conclusion and perspectives

Since 2003, both chemist and physicist communities worked hand in hand to design lanthanide-based SMMs, understand the mechanisms at the origin of their magnetic properties, and potentially drive the design of new target assemblies. Since few years, almost all the lanthanide ions were involved in such molecular species. In the present review we shed light on all existing examples to date of SMMs based not on the classical Dy^{III}, Tb^{III} and Er^{III} ions but on less commonly used lanthanides, *i.e.* Ce^{III}, Nd^{III}, Ho^{III}, Tm^{III} and Yb^{III} ions.

The ligands that have been employed up-to-now for their elaboration are of various natures with the presence of carboxylate, hydroxo, oxo, pyridine coordinating groups, macrocyclic ligands *etc*… illustrating the diversity in the chemical approaches and offering large perspective that may only be limited by chemists imagination. Nevertheless this review

highlights an efficient synthetic approach, *i.e.* organometallic synthesis, for all the lanthanide ions which allowed an efficient control of the crystal field around the lanthanide centre. Finally, two other strategies to obtain SMM with this kind of lanthanide ions were already successful: i) the insertion of diamagnetic ions such as Zn^{II} which add an electrostatic effect on the active centre and ii) the doping of the active SMM with a second 4*f* element.

On the magnetic point of view, the mechanisms at play in the slow magnetic relaxation seems to be more complicated than for the Tb^{III} and Dy^{III} SMMs since the Orbach process is not the main pathway of relaxation and should be discarded to the advantage of other processes such as Direct, Raman and Quantum pathways. These additional processes for the magnetic relaxation are at the origin of the discrepancy between the effective energy barriers extracted from ac and dc measurements, ab initio calculations and luminescence spectra. Thus to better understand the magnetic properties of such molecular edifices, the combination of several methods are crucial *i.e.* the evaluation of the crystal field splitting from dc magnetic data using Stevens operators, *ab-initio* calculations in support to the experimental results, and the correlation between luminescence and magnetism.

Despite the significant magnetic anisotropy highlighted by the reviewed SMMs, pure Ising system is not yet reached since the remaining transversal components induce QTM. This is induced by the mixing of the M_I states due to the intense hyperfine coupling and/or dipole-dipole interactions. Consequently new perspective can be envisioned for such complexes since they may be seen as good candidates for molecular spintronics.

References

[1] A. Caneschi, D. Gatteschi, R. Sessoli, A.-L. Barra, L. C. Brunel, M. Guillot, J. Am. Chem. Soc. 113 (1991) 5873.

[2] R. Sessoli, D. Gatteschi, A. Caneschi, M. A. Novak, Nature 365 (1993) 141.

[3] T. Lis, Acta Crystallogr. Sect. B 36 (1980) 2042.

[4] N. Ishikawa, M. Sugita, T. Ishikawa, S. Koshihara, Y. Kaizu, J. Am. Chem. Soc. 125 (2003) 86948695.

[5] B. J. Figgis Introduction to Ligand Fields, Wiley, New York, (1966).

[6] J. D. Rinehart, J. R. Long, Chem. Sci. 2 (2011) 2078.

[7] D. N. Woodruff, R. E. P. Winpenny, R. A. Layfield, Chem. Rev. 113 (2013) 5110.

[8] H. L. C. Feltham, S. Brooker, Coord. Chem. Rev. 276 (2014) 1.

[9] P. Zhang, Y.-N. Guo, J. Tang, Coord. Chem. Rev. 257 (2013) 1728.

[10] F. Pointillart, B. Le Guennic, O. Cador, O. Maury, L. Ouahab, Acc. Chem. Res. 48 (2015) 2834.

[11] S. T. Liddle, J. van Slageren, Chem. Soc. Rev. 44 (2015) 6655.

[12] F. Pointillart, K. Bernot, S. Golhen, B. Le Guennic, T. Guizouarn, L. Ouahab, O. Cador, Angew. Chem. Int. Ed. 54 (2015) 1504.

[13] Y.-N. Guo, G.-F. Xu, P. Gamez, L. Zhao, S.-Y. Lin, R. Deng, J. Tang, H.-J. Zhang, J. Am. Chem. Soc. 132 (2010) 8538.

[14] Y.-N. Guo, G.-F. Xu, W. Wernsdorfer, L. Ungur, Y. Guo, J. Tang, H.-J. Zhang, L. F. Chibotaru, A. K. Powell, J. Am. Chem. Soc. 133 (2011) 11948.

[15] S.-Y. Lin, W. Wernsdorfer, L. Ungur, A. K. Powell, Y.-N. Guo, J. Tang, L. Zhao, L. F. Chibotaru, H.-J. Zhang, Angew. Chem. Int. Ed. 51 (2012) 12767.

[16] Y.-N. Guo, L. Ungur, G. E. Granroth, A. K. Powell, C. Wu, S. E. Nagler, J. tang, L. F. Chibotaru, D. Cui, Sci. Rep. 4 (2014) 5471.

[17] R. A. Layfield, Organometallics 33 (2014) 1084.

[18] Y.-N. Guo, G.-F. Xu, Y. Guo, J. Tang, Dalton Trans. 40 (2011) 9953.

[19] P. Zhang, L. Zhang, J. Tang, Dalton Trans. 44 (2015) 3923.

[20] L. Ungur, S.-Y. Lin, J. Tang, L. F. Chibotaru, Chem. Soc. Rev. 43 (2014) 6894.

[21] R. Sessoli, A. K. Powell, Coord. Chem. Rev. 2009, 253, 2328 and references therein.

[22] S. Demir, I.-R. Jeon, J. R. Long, T. D. Harris, Coord. Chem. Rev. 289-290 (2015) 149 and references therein.

[23] K. Liu, W. Shi, P. Cheng, Coord. Chem. Rev. 289-290 (2015) 74.

[24] M. A. AlDamen, S. Cardona-Serra, J. M. Clemente-Juan, E. Coronado, A. Gaita-Arino, C. Marti-Gastaldo, F. Luis, O. Montero, Inorg. Chem. 48 (2009) 3467.

[25] B. S. Bassil, M. H. Dickman, B. Von der Kammer, U. Kortz, Inorg. Chem. 46 (2007) 2452.

[26] K. W. H. Stevens, Proc. Phys. Soc. A 65 (1952) 209.

[27] R. Orbach, Proc. Phys. Soc. A 264 (1961) 458.

[28] C. Rudowicz, J. Phys. C: Solid State Phys. 18 (1985) 1415.

[29] S. Liu, L.-W. Tang, S. Rettig, C. Orvig, Inorg. Chem. 32 (1993) 2773.

[30] F. Rived, M. Rosés, E. Bosh, Anal. Chim. Acta 374 (1998) 309.

[31] J.-L. Liu, K. Yuan, J.-D. Leng, L. Ungur, W. Wernsdorfer, F.-S. Guo, L. F. Chibotaru, M.-L. Tong, Inorg. Chem. 51 (2012) 8538.

[32] C. Görller-Walrand, K. Binnemans, Rationalization of Crystal-Field parametrization. In Handbook on the Physics and Chemistry of rare Earths; K. A. Jr. Gschneidner, L. Eyring, Eds. Elsevier: Amsterdam 23 (1996) 121.

[33] H. Schilder, H. Lueken, J. Magn. Magn. Mater. 281 (2004) 17.

[34] N. Ishikawa, M. Sugita, T. Ishikawa, S. Koshihara, Y. Kaizu, J. Phys. Chem. B 108 (2004) 11264.

[35] A. Abragam, B. Bleaney, Electron Paramagnetic Resonance of Transition Ions; Clarendon Press: Oxford, 1970.

[36] R. L. Carlin, Magnetochemistry; Springer-Verlag: New york, 1986.

[37] R. L. Carlin, A. J. van Duyneveldt, Magnetic Properties of Transition Metal Compounds; Springer-Verlag: New York 1977.

[38] A. Singh, K. N. Shrivastava, Phys. Status Solidi B 95 (1979) 273.

[39] K. N. Shrivastava, Phys. Status Solidi B 117 (1983) 437.

[40] W. Wernsdorfer, N. E. Chakov, G. Christou, Phys. Rev. B 70 (2004) 132413.

[41] W. Wernsdorfer, Adv. Chem. Phys. 118 (2001) 99.

[42] S.-Y. Lin, C. Wang, L. Zhao, J. Wua, J. Tang, Dalton Trans. 44 (2015) 223.

[43] J. Long, J. Rouquette, J.-M. Thibaud, R. A. S. Ferreira, L. D. Carlos, B. Donnadieu, V. Vieru, L. F. Chibotaru, L. Konczewicz, J. Haines, Y. Guari, J. Larionova, Angew. Chem., Int. Ed. 54 (2015) 2236.

[44] X.-L. Li, C.-L. Chen, H.-P. Xiao, A.-L. Wang, C.-M. Liu, X. Zheng, L.-J. Gao, X.-G. Yanga, S.-M. Fang, Dalton Trans. 42 (2013) 15317.

[45] K. Soussi, J. Jung, F. Pointillart, B. Le Guennic, B. Lefeuvre, S. Golhen, O. Cador, Y. Guyot, O. Maury, L. Ouahab, Inorg. Chem. Front. 2 (2015) 1105.

[46] M. Llunell, D. Casanova, J. Cirera, J. M. Bofill, P. Alemany, S. Alvarez, S. SHAPE (Version 2.1), Barcelona, 2013.

[47] J. Jung, O. Cador, K. Bernot, F. Pointillart, J. Luzon, B. Le Guennic, Beilstein J. Nanotechnol. 5 (2014) 2267.

[48] P. Goldner, F. Pellé, D. Meichenin, F. Auzel, J. Lumin. 71 (1997) 137.

[49] G. Zucchi, R. Scopelliti, P.-A. Pittet, J. C. G. Bünzli, R. D. Rogers, J. Chem. Soc., Dalton trans. (1999) 931.

[50] M. Sugita, N. Ishikawa, T. Ishikawa, S. Koshihara, Y. Kaizu, Inorg. Chem. 45 (2006) 1299.

[51] M. E. Boulon, G. Cucinotta, J. Luzon, C. Degl'Innocenti, M. Perfetti, K. Bernot, G. Calvez, A. Caneschi, R. Sessoli, Angew. Chem. Int. Ed. 52 (2013) 350.

[52] X. Yi, K. Bernot, V. Le Corre, G. Calvez, F. Pointillart, O. Cador, B. Le Guennic, J. Jung, O. Maury, V. Placide, Y. Guyot, T. Roisnel, C. Daiguebonne, O. Guillou, Chem. Eur. J. 20 (2014) 1569.

[53] F. Silva, O. L. Malta, C. Reinhard, H. U. Gudel, C. Piguet, J. E. Moser, J. C. G. Bunzli, J. Phys. Chem. A 106 (2002) 1670.

[54] C. Reinhard, H. U. Gudel, Inorg. Chem. 41 (2002) 1048.

[55] W. Huang, D. Wu, D. Guo, X. Zhu, C. He, Q. Meng, C. Duan, Dalton Trans. (2009) 2081.

[56] W. Huang, J. Xu, D. Wu, X. Huang, J. Jiang, New. J. Chem. 39 (2015) 8650.

[57] K. S. Pedersen, J. Dreiser, H. Weihe, R. Sibille, H. V. Johannesen, M. A. Sorensen, B. E. Nielsen, M. Sigrist, H. Mutka, S. Rols, J. Bendix, S. Piligkos, Inorg. Chem. 54 (2015) 7600.

[58] P. V. Bernhardt, B. M. Flanagan, M. Riley, Aust. J. Chem. 53 (2000) 229.

[59] K. S. Pedersen, L. Ungur, M. Sigrist, A. Sundt, M. Schau-Magnussen, V. Vieru, H. Mutka, S. Rols, H. Weihe, O. Waldmann, L. F. Chibotaru, J. Bendix, J. Dreiser, Chem. Sci. 5 (2014) 1650.

[60] B. M. Flanagan, P. V. Bernhardt, E. R. Krausz, S. R. Lüthi, M. J. Riley, Inorg. Chem. 41 (2002) 5024.

[61] E. Lucaccini, L. Sorace, M. Perfetti, J.-P. Costes, R. Sessoli, Chem. Commun. 50 (2014) 1648.

[62] M. Perfetti, E. Lucaccini, L. Sorace, J.-P. Costes, R. Sessoli, Inorg. Chem. 54 (2015) 3090.

[63] F. Pointillart, B. Le Guennic, S. Golhen, O. Cador, O. Maury, L. Ouahab, Chem. Commun. 49 (2013) 615.

[64] P.-H. Lin, W.-B. Sun, Y.-M. Tian, P.-F. Yan, L. Ungur, L. F. Chibotaru, M. Murugesu, Dalton Trans. 41 (2012) 12349.

[65] T.-Q. Liu, P.-F. Yan, F. Luan, Y.-X. Li, J.-W. Sun, C. Chen, F. Yang, H. Chen, X.-Y. Zou, G.-M. Li, Inorg. Chem. 54 (2015) 221.

[66] A. B. Castro, J. Jung, S. Golhen, B. Le Guennic, L. Ouahab, O. Cador, F. Pointillart, Magnetochemistry 2 (2016) 26.

[67] J. J. Le Roy, I. Korobkov, J. E. Kim, E. J. Schelter, M. Murugesu, Dalton Trans. 43 (2014) 2737.

[68] A. Ben Khélifa, M. Salah Belkhiria, G. Huang, S. Freslon, O. Guillou, K. Bernot, Dalton Trans. 44 (2015) 16458.

[69] J. J. Le Roy, M. Jeletic, S. I. Gorelsky, I. Korobkov, L. Ungur, L. F. Chibotaru, M. Murugesu, J. Am. Chem. Soc. 135 (2013) 3502.

[70] A. Ben Khélifa, M. Giorgi, M.-S. Belkhiria, Acta Crystallogr., Sect. E: Struct. Rep. Online 68 (2012) m938.

[71] W. G. Klemperer, W. Shum, J. Am. Chem. Soc. 98 (1976) 8291.

[72] S. Faulkner, S. J. A. Pope, B. P. Burton-Pye, Appl. Spectrosc. Rev. 39 (2004) 1.

[73] N. Magnani, C. Apostolidis, A. Morgenstern, E. Colineau, J.-C. Griveau, H. Bolvin, O. Walter, R. Caciuffo, Angew. Chem., Int. Ed. 50 (2011) 1696.

[74] J. J. Le Roy, S. I. Gorelsky, I. Korobkov, M. Murugesu, Organomettalics 34 (2015) 1415.

[75] C. Apostolidis, J. Rebizant, B. Kanellakopulos, R. von Ammon, E. Dornberger, J. Müller, B. Powietzka, B. Nuber, Polyhedron 16 (1997) 1057.

[76] J. D. Rinehart, J. R. Long, Dalton Trans. 41 (2012) 13572.

[77] H. Reddmann, C. Apostolidis, O. Walter, H.-D. Amberger, Z. Anorg. Allg. Chem. 632 (2006) 1405.

[78] J. Long, F. Habib, P.-H. Lin, I. Korobkov, G. Enright, L. Ungur, W. Wernsdorfer, L. F. Chibotaru, M. Murugesu, J. Am. Chem. Soc. 133 (2011) 5319.

[79] K. R. Meihaus, J. D. Rinehart, J. R. Long, Inorg. Chem. 50 (2011) 8484.

[80] P.-H. Lin, T. J. Burchell, R. Clérac, M. Murugesu, Angew. Chem., Int. Ed. 47 (2008) 8848.

[81] S.-D. Jiang, B.-W. Wang, G. Su, Z.-M. Wang, S. Gao, Angew. Chem., Int. Ed. 49 (2010) 7448.

[82] F. Luis, M. J. Martinez-Pérez, O. Montero, E. Coronado, S. Cardona-Serra, C. Marti-Gastaldo, J. M. Clemente-Juan, J. Sesé, D. Drung, T. Schurig, Phys. Rev. B: Condens. Matter 82 (2010) 060403.

[83] R. A. Layfield, J. J. W. McDouall, S. A. Sulway, F. Tuna, D. Collison, R. E. P. Winpenny, Chem. Eur. J. 16 (2010) 4442.

[84] P.-E. Car, M. Perfetti, M. Mannini, A. Favre, A. Caneschi, R. Sessoli, Chem. Commun. 47 (2011) 3751.

[85] G. Cosquer, F. Pointillart, S. Golhen, O. Cador, L. Ouahab, Chem. Eur. J. 19 (2013) 7895.

[86] T. T. da Cunha, J. Jung, M.-E. Boulon, G. Campo, F. Pointillart, C. L. M. Pereira, B. Le Guennic, O. Cador, K. Bernot, F. Pineider, S. Golhen, L. Ouahab, J. Am. Chem. Soc. 135 (2013) 16332.

[87] G. Cosquer, F. Pointillart, J. Jung, B. Le Guennic, S. Golhen, O. Cador, Y. Guyot, A. Brenier, O. Maury, L. Ouahab, Eur. J. Inorg. Chem. (2014) 69.

[88] J. J. Baldovi, J. M. Clemente-Juan, E. Coronado, A. Gaita-Arino, Polyhedron 66 (2013) 39.

[89] J. J. Baldovi, J. J. Borras-Almenar, J. M. Clemente-Juan, E. Coronado, A. Gaita-Arino, Dalton Trans. 41 (2012) 13705.

[90] P. Erdös, H. A. Razafimandimby, J. Phys. 40 (1979) C4.

[91] A. Arauzo, A. Lazarescu, S. Shova, E. Bartolomé, R. Cases, J. Luzon, J. Bartolomé, C. Turta, Dalton Trans. 43 (2014) 12342.

[92] S. G. Shova, Y. A. Simonov, M. Gdaniec, G. V. Novitchi, A. Lazarescu, K. I. Turta, Russ. J. Inorg. Chem. 47 (2002) 946.

[93] R. H. Ruby, H. Benoit, C. D. Jeffies, Phys. Rev. 127 (1962) 51.

[94] A. K. Jassal, N. Aliaga-Alcalde, M. Corbella, D. Aravena, E. Ruiz, G. Hundal, Dalton Trans. 44 (2015) 15774.

[95] J. Lehmann, A. Gaita-Arino, E. Coronado, D. Loss, J. Mater. Chem. 19 (2009) 1672.

[96] N. Ishikawa, M. Sugita, W. Wernsdorfer, J. Am. Chem. Soc. 27 (2005) 3650.

[97] N. Ishikawa, M. Sugita, T. Okubo, N. Tanaka, T. Iino, Y. Kaizu, Inorg. Chem. 42 (2003) 2440.

[98] A. De Cian, M. Moussavi, J. Fischer, R. Weiss, Inorg. Chem. 24 (1985) 3162.

[99] H. Konami, M. Hatano, A. Tajiri, Chem. Phys. Lett. 160 (1989) 163.

[100] R. D. Shannon, Acta Crystallogr., Sect. A 32 (1976) 751.

[101] S. Qhosh, S. Datta, L. Friend, S. Cardona-Serra, A. Gaita-Arino, E. Coronado, S. Hill, Dalton Trans. 41 (2012) 13697.

[102] S. Cardona-Serra, J. M. Clemente-Juan, E. Coronado, A. Gaita-Arino, A. Camon, M. Evangelesti, F. Luis, M. J. Martinez-Perez, J. Sesé, J. Am. Chem. Soc. 134 (2012) 14982.

[103] R. J. Blagg, F. Tuna, E. J. L. McInnes, R. E. P. Winpenny, Chem. Commun. 47 (2011) 10587.

[104] T. Fukuda, N. Shigeyoshi, T. Yamamura, N. Ishikawa, Inorg. Chem. 53 (2014) 9080.

[105] C. R. Ganivet, B. Ballesteros, G. De la Torre, J. M. Clemente-Juan, E. Coronado, T. Torres, Chem. Eur. J. 19 (2013) 1457.

[106] D. I. Alexandropoulos, L. Cunha-Silva, L. Pham, V. Bekiari, G. Christou, T. C. Stamatatos, Inorg. Chem. 53 (2014) 3220.

[107] S. Yamauchi, T. Fujinami, N. Matsumoto, N. Mochida, T. Ishida, Y. Sunatsuki, M. Watanabe, M. Tsuchimoto, C. Coletti, N. Re, Inorg. Chem. 53 (2014) 5961.

[108] S. Thiele, F. Balestro, R. Ballou, S. Klyatskaya, M. Ruben, W. Wernsdorfer, Science 344 (2014) 1135.

[109] S.-D. Jiang, B.-W. Wang, H.-L. Sun, Z.-M. Wang, S. Gao, J. Am. Chem. Soc. 133 (2011) 4730.

[110] K. R. Meihaus, J. R. Long, J. Am. Chem. Soc. 135 (2013) 17952.

[111] P. Zhang, L. Zhang, C. Wang, S. Xue, S.-Y. Lin, J. Tang, J. Am. Chem. Soc. 136 (2014) 4484.

[112] J. J. Le Roy, I. Korobkov, M. Murugesu, Chem. Commun. 50 (2014)1602-1604.

[113] S.-D. Jiang, S.-S. Liu, L.-N. Zhou, B.-W. Wang, Z.-M. Wang, S. Gao, Inorg. Chem. 51 (2012) 3079.

[114] S. Cardona-Serra, J. M. Clemente-Juan, E. Coronado, A. Gaita-Arino, A. Camon, M. Evangelisti, F. Luis, M. J. Martinez-Pérez, J. Sesé, J. Am. Chem. Soc. 134 (2012) 14982.

[115] J. Ruiz, G. Lorusso, M. Evangelisti, E. K. Brechin, S. J. A. Pope, E. Colacio, Inorg. Chem. 53 (2014) 3586.

[116] Y.-S. Meng, Y.-S. Qiao, B.-W. Wang, Y.-Q. Zhang , S.-D. Jiang, Z.-S. Meng, B.-W. Wang, Z.-M. Wang, S. Gao, Chem. Eur. J. 22 (2016) 4704.

[117] H.-D. Amberger, F; T. Edelmann, J. Gottfriedsen, R. Herbst-Irmer, S. Jank, U. Kilimann, M. Noltemeyer, H. Reddmann, M. Schäfer, Inorg. Chem. 48 (2008) 760.

[118] K. S. Pedersen, A.-M. Ariciu, S. McAdams, H. Weihe, J. Bendix, F. Tuna, S. Piligkos, J. Am. Chem. Soc. 138 (2016) 5801.

[119] M. Atzori, L. Tesi, E. Morra, M. Chiesa, L. Sorace, R. Sessoli, J. Am. Chem. Soc. 138 (2016) 2154.

[120] L. Tesi, E. Lucaccini, I. Cimatti, M. Perfetti, M. Mannini, M. Atzori, E. Morra, M. Chiesa, A. Caneschi, L. Sorace, R. Sessoli, Chem. Sci. 7 (2016) 2074.

[121] M. S. Fataftah, S. C. Coste, B. Vlaisavljevich, J. M. Zadrozny, D. E. Freedman, Chem. Sci. 7 (2016) 6160.

[122] M. Shiddiq, D. Komijani, Y. Duan, A. Gaita-Arino, E. Coronado, S. Hill, Nature 531 (2016) 348.

[123] A. Fernandez, J. Ferrando-Soria, E. M. Pineda, F. Tuna, I. J. Vitorica-Yrezabal, C. Knappke, J. Ujma, C. A. Muryn, G. A. Timco, P. E. Barran, A. Ardavan, R. E. P. Winpenny Nature Commun. 7 (2016) 1.

[124] Q.-W. Li, J.-L. Liu, J.-H. Jia, Y.-C. Chen, J. Liu, L.-F. Wang, M.-L. Tong, Chem. Commun. 51 (2015) 10291.

[125] M. S. Lah, V. L. Pecoraro, J. Am. Chem. Soc. 111 (1989) 7258.

[126] J. J. Bodwin, A. D. Cutland, R. G. Malkani, V. L. Pecoraro, Coord. Chem. Rev. 216-217 (2001) 489.

[127] G. Mezei, C. M. Zaleski, V. L. Pecoraro, Chem. Rev. 107 (2007) 4933.

[128] J. Jankolovits, J. W. Kampf, V. L. Pecoraro, Inorg. Chem. 53 (2014) 7534.

[129] H. L. C. Feltham, F. Klöwer, S. A. Cameron, D. S. Larsen, Y. Lan, M. Tropiano, S. Faulkner, A. K. Powell, S. Brooker, Dalton Trans. 40 (2011) 11425.

[130] C. Lampropoulos, S. Hill, G. Christou, ChemPhyschem 10 (2009) 2397.

[131] J. Ruiz, G. Lorusso, M. Evangelesti, E. K. Brechin, S. J. A. Pope, E. Colacio, Inorg. Chem. 53 (2014) 3586.

[132] S. Hino, M. Maeda, K. Yamashita, Y. Kataoka, M. Nakano, T. Yamamura, H. Nojiri, M. Kofu, O. Yamamuro, T. Kajiwara, Dalton Trans. 42 (2013) 2683.

[133] S. K. Singh, T. Gupta, L. Ungur, G. Rajaraman, Chem. Eur. J. 21 (2015) 13812.

[134] J.-D. Leng, J.-L. Liu, Y.-Z. Zheng, L. Ungur, L. F. Chibotaru, F.-S. Guo, M.-L. Tong, Chem. Commun. 49 (2013) 158.

[135] Q.-W. Li, J.-L. Liu, J.-H. Jia, J.-D. Leng, W.-Q. Lin, Y.-C. Chen, M.-L. Tong, Dalton Trans. 42 (2013) 11262.